SUPPLEMENTAL MATERIAL

Supplemental Methods

The data and methods that support the findings of this study are available from the corresponding author upon reasonable request.

Studies involving experimental animals

Generation of mice

Mice with platelet-specific deletion of transforming growth factor beta 1 (Plt.TGFβ) were generated, as described.[1] To generate mice with inducible, endothelial-specific deletion of TGFβRII, mice with loxP-flanked (floxed, flox/flox) TGFβRII locus[2] were mated with transgenic mice expressing a tamoxifen-inducible Cre recombinase-estrogen receptor ER^{T2} fusion protein under control of the endothelial receptor tyrosine kinase (Tie2) promoter (courtesy of Bernd Arnold).[3] Mice expressing a green fluorescent reporter gene under control of the Tie2.Cre^{ERT2} promoter were generated earlier.[4] Genotyping was performed using genomic DNA isolated from tail biopsies and primers shown in Online Table I. Cre recombinase activity was induced by feeding 5-weeks-old mice rodent chow containing tamoxifen citrate (TD55125; Harlan Teklad).[3] Age- and sex-matched littermates were used throughout the study. Mice were assigned a numerical code to ensure that experiments are carried out in a blinded manner. At baseline, mice with platelet-specific TGFβ deletion or endothelial-specific TGFβRII deletion did not phenotypically differ from their wild-type littermates and were born at the expected Mendelian ratio. We also did not observe any gross phenotypic or behavioral abnormalities, changes in body weight or increased mortality.

Induction of venous thrombosis and pulmonary embolism

Venous thrombosis was induced in male mice (12-14 weeks-of-age) by subtotal ligation of the *inferior Vena cava* (IVC) using a 5-0 Prolene suture (Ethicon) placed as a spaceholder alongside the IVC, as described.[5] Side and back branches were not ligated. Surgical IVC ligation was performed by the same operateur blinded to the mouse genotype/treatment group. Mice were anesthetized by intraperitoneal injection of a mixture of midazolam (5.0 mg/kg body weight [BW]), medetomidine (0.5 mg/kg/BW) and fentanyl (0.05 mg/kg/BW). At the end of the procedure, sedation was reversed with atipemazol (0.05 mg/kg/BW) and flumazenile (0.01 mg/kg/BW). As analgesic, buprenorphine hydrochloride (0.075 mg/kg/BW) was subcutaneously injected immediately following the procedure and one day later. The following day, mice were anesthetized via 2.5% isoflurane inhalation and non-invasive hemodynamic measurements were performed to determine blood flow velocity and the extent of venous thrombosis (including imaging in 3-dimensional mode) using high frequency ultrasound (Vevo 3100; FujiFilm, VisualSonics) and a 55 MHz mouse scanhead (FujiFilm, VisualSonics). In some animals, bosentan (Tocris; 5 mg/kg BW) was administered via intraperitoneal injection, beginning at day 1 after surgery and once per week thereafter until sacrifice at day 21, as published before.[6,7] Mice injected with vehicle alone were used as control. Littermate mice were randomly assigned to the control or treatment group. Only animals which had formed a thrombus were included in the study. Three weeks after surgery, the IVC was harvested from anesthetized mice and either paraffin embedded and processed for histological analysis or digested and prepared for flow cytometry. To examine the presence of pulmonary emboli, lungs were carefully perfused with PBS and infusion-fixed (via the trachea) with zinc formalin.[8] Serial paraffin-embedded cross-sections were stained using Carstairs' to simultaneously detect fibrin, platelets and fibrosis or monoclonal antibodies to visualize fibrinogen (abcam; ab189490) or platelets (CD41; exbio; 11-763-C100). TGFβ1 was detected using monoclonal antibodies (Novus Biologicals; MAB240). The

number of pulmonary arteries and arterioles occluded by fibrin-rich material was manually quantified per microscopic field (at X200 magnification).

All experiments involving animals had been approved by the Animal Research Committee of the University of Mainz and the authorities of Rhineland-Palatine and complied with national guidelines for the care and use of laboratory animals.

Enzyme-linked immunoassay

Plasma levels of active TGFβ1, plasminogen activator inhibitor-1 (PAI-1), endothelin-1 (ET-1) and platelet factor 4 (PF4) were determined using enzyme-linked immunoassay (TGFβ1 from R&D Systems; PAI-1, ET-1 and PF4 from abcam). To activate TGFβ1, one volume was calcified with 0.2 volume of 1 N HCl and incubated for 10 min at room temperature followed by neutralization with 0.2 volume of 1.2 N NaOH in 0.5 M HEPES buffer.

Aortic ring assay

The mouse aortic ring assay was performed, as published.[9] Briefly, murine aortas were cut into 2 mm-sized pieces, embedded in either matrigel™ or collagen type I (both Corning) and cultivated for four days in Endothelial Cell Growth Medium MV2 kit (PromoCell). In some experiments, SB431542 (10 µM; to block ALK5, but also ALK4 and ALK7;[10] Tocris), K02288 (10 µM; to block ALK1, but also ALK2 and ALK6;[11] Selleckchem) or bosentan monohydrate (10 µM; to block endothelin receptor-dependent signaling; Tocris) were added. Brightfield images were taken using a phase-contrast microscope (Zeiss Z1) equipped with a camera (Motic AE31). Aortic rings were fixed in 4% paraformaldehyde (PFA) and stained with Texas Red-labeled *Lycopersicum Esculentum* lectin (LEL; Vector) and antibodies against murine smooth muscle α-actin (SMA; Sigma-Aldrich) or fibroblast-specific protein-1 (FSP-1; Novus Biologicals).

Studies using murine platelets

Blood collection, platelet counts and preparation of platelet-rich plasma (PRP)

Blood was collected by cardiac puncture and anticoagulated with sodium citrate (3.8 %) and platelet counts were determined within 20 minutes after blood collection using an Automated Hematology Analyzer (KX-21N; Sysmex). PRP was obtained by centrifugation of citrated blood, undiluted for 2 min at 200 x g (room temperature) for platelet aggregation experiments and diluted 1:1 with Tyrode buffer (pH 7.4) for 4 min at 100 x g (room temperature) for flow cytometry analysis as described.[12]

Flow cytometry analysis

To 100 µL of diluted PRP, platelet agonists (i.e. ADP; Sigma Aldrich, A2754) at a concentration of 0.5, 1.0 and 2.5 µM and α-thrombin (Sigma-Aldrich; T6624) at a concentration of 0.03, 0.075 and 0.3 U/mL were added and incubated for 6 min at room temperature. Fluorescent-conjugated primary antibody (JON/A-PE; Emfret, D200) was incubated for 20 min. Finally, 500 µL Tyrode buffer (pH 7.4) was added, and samples were directly measured on FACs Canto II (BD Biosciences).[13]

Light transmission aggregometry

PRP was adjusted to 2 x 10^8 platelets per mL with Tyrode buffer, pH 7.4. Platelet aggregation was induced by 0.1 U/mL thrombin in the presence of the fibrin-polymerization inhibiting peptide GPRP (5 mM, Bachem, H-2935) and monitored at 37°C over a 7-minute time period under stirring (1000 s^{-1}) in a photometric aggregometer (Apact 4S Plus; DiaSys Germany).[14] To examine possible role of ET-1 and TGFβ1 in platelets aggregation PRP from C57BL/6 mice was collected and pre-incubated with ET-1 (1 µM; EnzoLifeSciences, ALX-155-001-PC01) and TGFβ1 (10 ng/mL; eBioscience, 14-8348-62) at 37°C for 10 min and platelet

aggregation was induced using α-thrombin (0.1 U/mL; Sigma-Aldrich; T6624) and convulxin (5 ng/mL; EnzoLifeSciences, ALX-350-100-C050).

Studies using primary endothelial cells

Isolation and cultivation

Human Umbilical Vein Endothelial Cells (HUVECs, PromoCell), Human Pulmonary Arterial Endothelial Cells (HPAECs, ATCC), Human Pulmonary Vein Endothelial Cells (HPVECs, CellBiologics) and endothelial cells outgrown from PEA tissue (CTEPH-ECs) were cultivated according to the protocol of the supplier and as published.[15] Mouse primary endothelial cells (mPECs) were isolated from lungs, as described.[4]

Immunofluorescence and confocal microscopy

Cells were plated onto coverslips pre-coated with 0.2% gelatin (Sigma) at 37°C under 5% CO_2 and cultivated in Endothelial Cell Growth Medium MV2 kit (PromoCell). Following fixation with 4% PFA, cells were permeabilized using 0.2% Triton X-100 (in PBS; Roth) for 5 min. Unspecific antigen binding was blocked using 5% normal serum. Primary antibodies to detect VE-cadherin (CDH5; abcam; ab33168), ALK1 (Novus Biologicals; NBP1-30982), ALK5 (abbiotec; 250879), endothelin-1 (ET-1; ThermoFisher; PA3-067), SMA (abcam; ab15267), CD41 (exbio; 11-763-C100) or TGFβ1 (Novus Biologicals; MAB240) were incubated for 45 min followed by incubation with AlexaFluor FITC- (Invitrogen; 18746), AlexaFluor 647- (Molecular Probes; A21245), MFP488- or MFP555- (MoBiTec; MFP-A1008 and MFP-A2428, respectively) conjugated secondary antibodies. Isotype IgG controls (Dako; X0944 for mouse, X0936 for rabbit and Santa Cruz Biotechnology, sc-2026 for rat) were used to exclude unspecific background staining (Online Figure IIA and IIB). Cell nuclei were detected using 4',6-diamidin-2-phenylindol (DAPI; Roth; 6335.1). Images were

collected using a Leica LSM710 confocal microscope and analyzed using Leica software (LAS X).

Studies involving human tissue

Patient recruitment

Tissue specimens were obtained from patients diagnosed with CTEPH who underwent PEA surgery at the Kerckhoff Clinic, Department of Thoracic Surgery, Bad Nauheim, Germany. All patients with confirmed CTEPH transferred for PEA were eligible for the study; only patients who refused or withdrew consent were excluded. Following PEA, tissues were placed in Dulbecco's Modified Eagle's Medium (DMEM) containing high glucose (Gibco), immediately transferred on ice to our laboratory and processed for subsequent analysis, as described. The study was approved by the local ethics committee, and all patients gave written informed consent. Plasma samples used in the study were obtained from the *Mainz Registry for Pulmonary Hypertension* (PHYREM) at the University Medical Center Mainz, Germany. Out of 150 consecutive patients who had been prospectively enrolled in the registry at the time that plasma for the present study was requested, we selected samples (n=45 in total), which met specific requirements, such as: (i) plasma availability from three follow-up appointments; (ii) absence of HIV infection; (iii) absence of inflammatory disease; and (iv) absence of congenital heart disease. Of these patients, the diagnosis was chronic thromboembolic pulmonary hypertension (CTEPH) in 19 and pulmonary arterial hypertension in 26. Both studies were conducted in accordance with the amended Declaration of Helsinki and approved by the local ethics committee.

Histology

PEA specimens were fixed overnight in 4% zinc formalin, embedded in paraffin or cryo-preserved using Tissue-Tek® O.C.T. (Sakura® Finetek) and cut into 5 µm-thick serial cross

sections. Following modified Carstairs' stain to distinguish red blood cells (yellow), fibrin (orange-red) and platelets (grey), CTEPH specimens were classified into five distinct regions containing primarily fresh thrombi or organized thrombus, myofibroblasts, vessels or fibrosis, based on published criteria.[15] Interstitial collagen was detected using picrosirius red staining followed by polarization microscopy.

General methods

Flow cytometry analysis

Cells were fixed using 0.1% PFA followed by permeabilization using 0.1% Triton X-100 for 5 min. Unspecific binding was blocked using FcR receptor blocking reagent (Miltenyi Biotech; 130-092-575) followed by incubation with primary antibodies against SMA (Sigma-Aldrich; A2547), FSP1 (Novus Biologicals; NBP1-89402), CDH5 (abcam; ab33168), CD31-APC (BioLegend; 102510), TGFβRII (ThermoScientific; PA5-35076), TGFβRI/ALK5 (Abnova; PAB18420), TGFβRIII-AlexaFluor-647 (bioss; bs-1910R-647) and FGFR1 (Cell Signaling Technology; cst-9740). Unconjugated primary antibodies were followed by AlexaFluor488-conjugated secondary antibodies (Molecular Probes; A21311).

Quantitative real time polymerase chain reaction

Total RNA was isolated using Trizol® reagent (Ambion). One µg of RNA was treated with DNase I to eliminate genomic DNA, reversed transcribed into cDNA using iScript cDNA Synthesis Kit (BioRad) followed by quantitative *real time* PCR. All qPCR data are normalized to HPRT1 (for human) or 18S (for mouse) and are reported as -fold change vs. the control, as specified in the text. Primer sequences and PCR conditions are shown in Online Table II (human) and Online Table III (mouse).

Western blot

Cells were lyzed in RIPA buffer containing 1 mM PMSF (phenylmethanesulfonyl fluoride; Cell Signaling Technology). Equal amounts of protein were fractionated by SDS polyacrylamide gel electrophoresis together with molecular weight standards and transferred to nitrocellulose membrane (Protran®, Whatman). Membranes were blocked in 5% bovine serum albumin (in TBS/0.1% Tween-20) followed by incubation with primary antibodies against ET-1 (ThermoFisher; PA3-067). Antibodies against GAPDH (HyTest; 5G4 Mab 6C5) were used to demonstrate total protein loading. Protein bands were visualized using horseradish peroxidase-conjugated secondary antibodies (Amersham Biosciences; NA931 and NA934 against mouse or rabbit IgG, respectively) and detected with SuperSignal® West Pico Substrate (Pierce).

Immunohistochemistry

Immunohistochemistry was performed on 4% zinc formalin-fixed paraffin sections, as described.[15] For mouse thrombi, serial sections were used; for PEA specimens, tissue microarrays were prepared. Endothelial or mesenchymal cells were analyzed using antibodies against CD31 (Dianova; DIA-310), CDH5 (abcam; ab33168) or SMA (Sigma-Aldrich; A2547), FSP1 (Novus Biologicals; NBP1-89402) and DDR2 (Novus Biologicals; NBP2-14926). TGFβ signaling was analyzed using antibodies against TGFβRII (ThermoScientific; PA5-35076), TGFβRI/ALK5 (abbiotec; 250879), TGFβRI/ALK1 (Novus Biologicals; NBP1-30982), TGFβ1 (Novus Biologicals; NBP1-80289), phospho-SMAD2/3 (Millipore; AB3849), phospho-SMAD5 (abcam; ab92698) and ET-1 (ThermoFisher; PA3-067). Fibrinogen was detected using monoclonal antibodies (abcam; ab189490). All primary antibodies were incubated overnight at 4°C in a humid chamber. The next day, secondary antibodies were incubated for 1 hour followed by incubation with avidin-biotin peroxidase link (Vector Laboratories; BA-9400) and peroxidase substrate until color development. Sections were

counterstained with Gill's hematoxylin (Sigma) and mounted with ImmuMount (ThermoScientific). Sections were photographed on an Olympus BX51 microscope and analyzed using analysis software (Image ProPlus, version 7.04). Isotype IgG controls (Dako; X0944 for mouse, X0936 for rabbit and Santa Cruz, sc-2026 for rat) were used to exclude unspecific background staining (Online Figure IIC and IID). The number of phospho-SMAD2/3- or SMAD5-positive cells was manually counted and expressed as number of positive cells per microscope field (at X200 magnification). For all others, the intensity of the immunosignal was measured using the 'count-size' function and expressed as % positive area.

Statistical analysis

Quantitative data are presented as mean±standard error of the mean (SEM). Normal distribution was examined using the D'Agostino-Pearson omnibus normality test. For comparison of two groups and normal distribution, Student's t-test was performed. If more than two groups were compared, One-way ANOVA followed by Bonferroni's multiple comparisons test was performed. Multiple test correction across experiments was not performed. Non-parametric tests (Mann-Whitney and Kruskall-Wallis test) were used if normal distribution was not present. Statistical significance was assumed if P reached a value less than 0.05. All analyses were performed using GraphPad Prism version 7.04 for Windows (GraphPad Prism Software).

Online Tables

Online Table I. Genotyping primer sequences

Gene	Primer sequences (in 5‘ – 3‘ direction)	T_m (°C)	cycles	ref
Pf4.Cre	F: CCCATACAGCACACCTTTTG R: TGCACAGTCAGCAGGTT	60	35	E[16]
TGFβ flox	F: AAGACCTGGGTTGGAAGTG R: CTTCTCCGTTTCTCTGTCACCCTAT	60	35	E[1]
Tie2.ER^{T2}-Cre	F: CGAGTGATGAGGTTCGCAAG R: TGAGTGAACGAACCTGGTCG	58	35	E[3]
TGFβRII flox	F: GCACAGGTACACATCTCTGCAC R: TGTAATCGTTGCACTCTTCCATGT	56	30	E[2]
IRG flox	F: GCCGACATCCCCGACTAC R: GCTTCAGGGCCTTGTGGATCT	60	40	E[17]

Online Table II. Human primer sequences and qRT-PCR conditions

Gene	Primer sequences (in 5‘ – 3‘ direction)	T_m (°C)	cycles	ref
ACTA2	F: GACAGCTACGTGGGTGACGAA R: TTTTCCATGTCGTCCCAGTTG	60	40	E[18]
ALK1	F: ACTCACAGGGCAGCGATTAC R: CATTGGGCACCACATCATAG	60	40	E[19]
ALK5	F: TGTCATTGCTGGACCAGTGTG R: CAGTGCGGTTGTGGCAGATATA	60	40	E[20]
CDH5	F: TCACCTTCTGCGAGGATATGG R: GAGTTGAGCACCGACACATC	60	40	E[21]
COL1A1	F: CAGCCGCTTCACCTACAGC R: TTTTGTATTCAATCACTGTCTTGCC	60	40	E[22]
EDN1	F: GACATCATTTGGGTCAACACTC R: GGCATCTATTTTCACGGTCTGT	60	40	E[23]
ENG	F: GAATTCTGGTACATCTACTCGC R: GGCTATGCCATGCTGCTGGTGG	60	40	E[24]
FGFR1	F: AACCTGACCACAGAATTGGAGGCT R: ATGCTGCCGTACTCATTCTCCACA	60	40	E[25]
HPRT1	F: GTAATTGGTGGAGATGATCTCTCAACT R: TGTTTTGCCAGTGTCAATTATATCTTC	60	40	E[26]
PECAM1	F: AACAGTGTTGACATGAAGAGCC R: TGTAAAACAGCACGTCATCCTT	60	40	E[27]
SNAIL	F: GGCAATTTAACAATGTCTGAAAAGG R: GAATAGTTCTGGGAGACACATCG	60	40	E[28]

TGFB1	F: CCCAGCATCTGCAAAGCTC R: GTCAATGTACAGCTGCCGCA	60	40	E[29]
TGFBR2	F: GACCCCAAGCTCACCTACCA R: TGCACTCATCAGAGCTACAGGA	60	40	E[30]
TWIST	F: CTCAAGAGGTCGTGCCAATC R: CCCAGTATTTTTATTTCTAAAGGTGTT	60	40	E[28]
ZEB1	F: TTCAAACCCATAGTGGTTGCT R: TGGGAGATACCAAACCAACTG	60	40	E[31]

Online Table III. Mouse primer sequences and qRT-PCR conditions

Gene	Primer sequences (in 5‘ – 3‘ direction)	T_m (°C)	cycles	ref
18S	F: CGAAAGCATTTGCCAAGAAT R: GAGGTTTCCCGTGTTGAGTC	60	40	
Acta2	F: GGACGTACAACTGGTATTGTGC R: CGGCAGTAGTCACGAAGGAAT	60	40	E[32]
Alk1	F: GGCCTTTTGATGCTGTCG R: ATGACCCCTGGCAGAATG	60	40	E[33]
Alk5	F: TGTGCACCATCTTCAAAAACA R: ACCAAGGCCAGCTGACTG	60	40	E[33]
Angpt2	F: AGAAGCAGCAGCATGACC R: TGCCACTGGTGGTGAGTCC	60	40	E[34]
Bambi	F: AGCGCGAGGCGTCAATG R: GCAGGCACTAAGCTCAGACT	60	40	E[34]
Cdh5	F: GGCCCTGGACAGACTGCA R: TTCGTGGAGGAGCTGATC	60	40	E[35]
Col1a1	F: ATGGATTCCCGTTCGAGTACG R: TCAGCTGGATAGCGACATCG	60	40	E[36]
Edn1	F: TGAGTTCCATTTGCAACCGAGT R: CTGAGTTCGGCTCCCAAGAC	60	40	E[37]
Eng	F: AGCCCCACAAGTCTTGCAG R: GCTAGTGGTATATGTCACCTCGC	60	40	E[19]
Fgfr1	F: TGTTTGACCGGATCTACACACA R: CTCCCACAAGAGCACTCCAA	60	40	E[38]

Id1	F: TTGTTCTCTTCCCACACTCTGTTC R: CTGGCGACCTTCATGATCCT	60	40	E[39]
Mcp1	F: CTGTCTCAGCCAGATGCAGTTAA R: AGCCGACTCATTGGGATCAT	60	40	E[40]
Mmp2	F: GCCCCGAGACCGCTATGTCCACT R: GCCCCACTTCCGGTCATCATCGTA	60	40	E[41]
Mmp9	F: GAGCTGTGCGTCTTCCCCTTC R: GGAATGATCTAAGCCCAGTGC	60	40	E[42]
Notch1	F: AGGACGTGGATGAGTGTGCT R: CCCAGTGTGTTGAGGCATTT	60	40	E[43]
Pai1	F: GCTGTAGACGAGCTGACACG R: TAGGGCAGTTCCACAACGTC	60	40	E[44]
Pecam1	F: GCGCAGGACCACGTGTTAGT R: CCTGCAATTTGAATCCGGAC	60	40	E[36]
Snail	F: GTGCCCACCTCCAAACCC R: AAGGACATGCGGGAGAAGG	60	40	P
Tgfb1	F: CAGTGGCTGAACCAAGGAGAC R: ATCCCGTTGATTTCCACGTG	60	40	E[45]
Tgfbr2	F: AGCATCACGGCCATCTGTG R: TGGCAAACCGTCTCCAGAGT	60	40	E[46]
Twist	F: TGATAGAAGTCTGAACACTCGTTTG R: GGCTGATTGGCAAGACCTCT	60	40	P
uPA	F: TTACTGCAGGAACCCTGACAACCA R: TGCTAAGAGAGCAGTCATGCACCA	60	40	E[47]
Zeb1	F: GCTGGCAAGACAACGTGAAAG	60	40	E[48]

R: GCCTCAGGATAAATGACGGC

Online Table IV. Clinical and laboratory parameters in CTEPH patients at the time of surgery

	PAH	**CTEPH**	**P value**
patients (n)	**26**	**19**	
male sex (%)	10/26 (38.5%)	8/19 (42.1%)	1.000
age (years)	72 (68-88)	73 (61-83)	0.629
BMI	28 (26-30)	28 (23-30)	0.524
Comorbidities			
Renal insufficiency (%)	4/26 (15.4%)	4/19 (21.1%)	0.704
History of DVT (%)	2/26 (7.7%)	18/19 (94.7%)	**<0.001**
Coronary artery disease (%)	14/26 (53.8%)	3/19 (15.8%)	**0.013**
Diabetes mellitus (%)	8/26 (30.8%)	2/18 (11.1%)	0.161
Active cancer (%)	0/26 (0.0%)	1/19 (5.3%)	0.422
Functional capacity and imaging testing			
6 MWD (m)	364 (307-480) n=24	350 (275-450) n=16	0.633
systolic PAP in TTE (mmHg)	60 (50-85) n=25	60 (42-81) n=17	0.608
TAPSE in TTE (mm)	22 (17-25) n=24	20 (16-21) n=17	0.644
Medication			
Endothelin receptor antagonists (%)	20/26 (76.9%)	1/19 (5.3%)	**<0.001**
Phosphodiesterase type 5 inhibitors (%)	20/26 (76.9%)	5/19 (26.3%)	**0.001**
Prostacyclin analogues (%)	3/26 (11.5%)	0/20 (0.0%)	0.252
Soluble guanylate cyclase stimulators (%)	1/26 (3.8%)	8/19 (42.1%)	**0.002**

Abbreviations: *DVT*, deep vein thrombosis; *MWD*, minutes walk distance; *systolic PAP*, systolic pulmonary arterial pressure; *TAPSE*, tricuspid annular plane systolic excursion; *TTE*, transthoracic echocardiography

Online Figures

Online Figure I

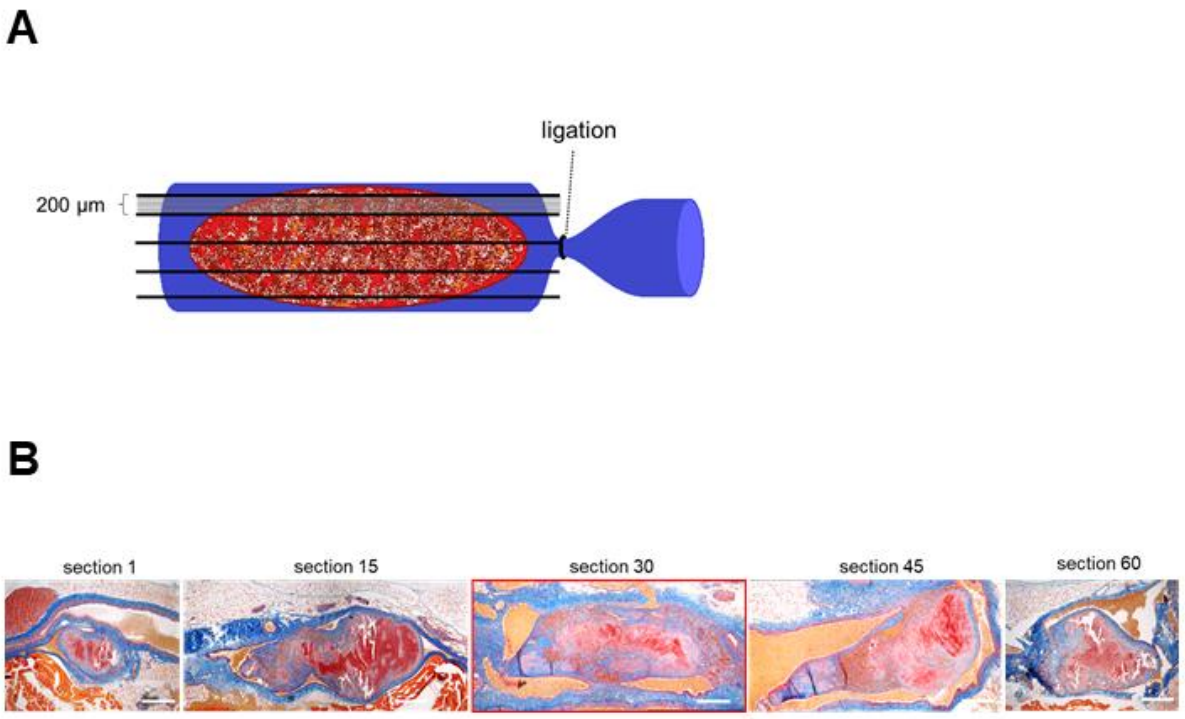

Online Figure I. Morphometric analysis of murine venous thrombi. Schematic representation of the thrombosed inferior Vena cava processed for serial longitudinal paraffin-embedded tissue sections equally spaced through the thrombosed vein segment (**A**). Exemplary results after Carstairs' staining of selected sections (approximately 200 µm apart) with the section containing the largest thrombus chosen for quantitative analysis highlighted by red borders (**B**). Scale bars represent 200 µm.

Online Figure II

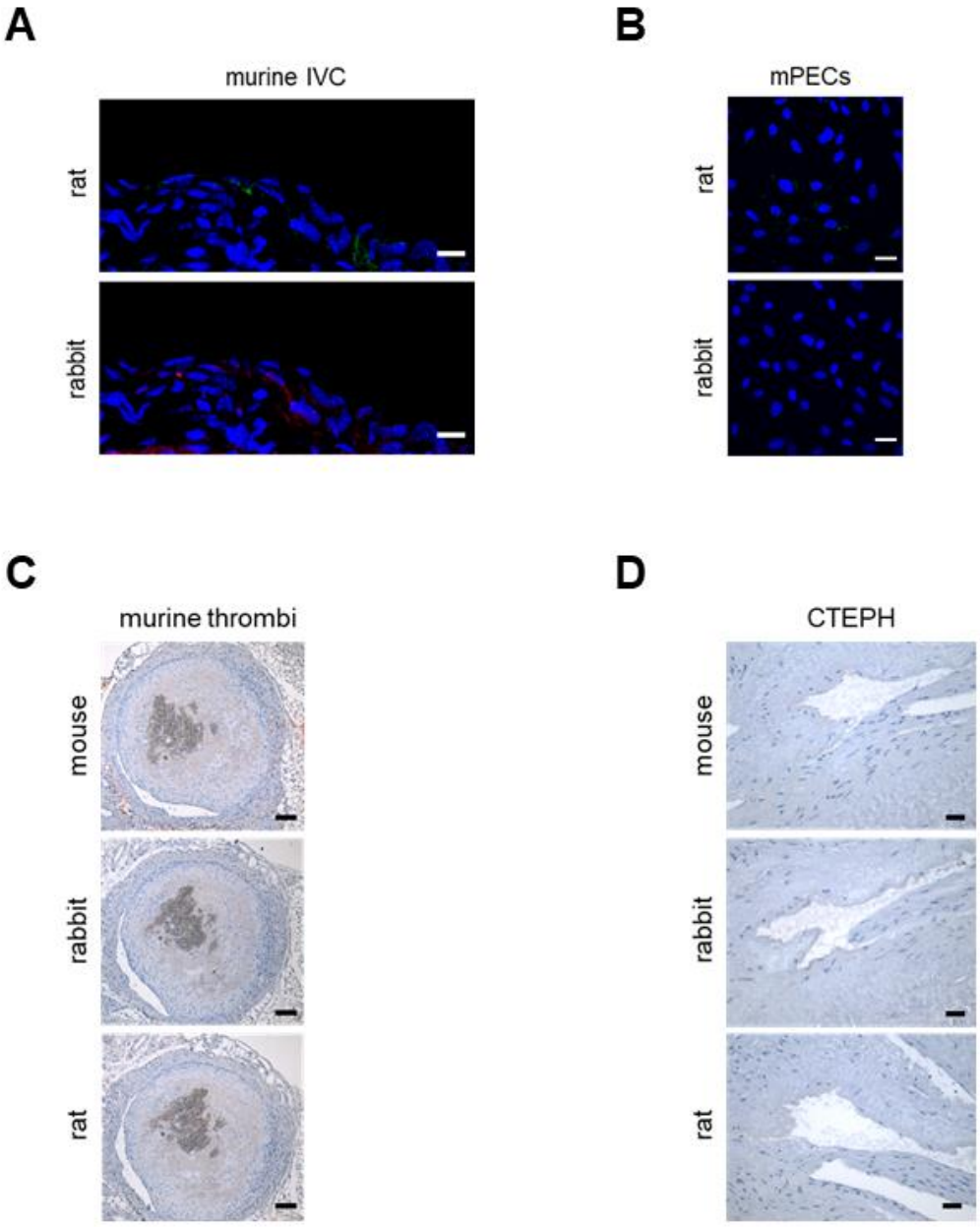

Online Figure II. Isotype controls used for immunofluorescence and immunohistochemical staining. Representative confocal microscopy images of the murine inferior Vena cava (IVC; **A**) and murine pulmonary endothelial cells (mPECs; **B**) in culture stained using rat and rabbit isotype controls. Representative images of mouse venous thrombi isolated at day 21 after IVC ligation (**C**) and of human CTEPH pulmonary endarterectomy specimens (**D**) stained using isotype IgG controls from mouse, rabbit or rat. Scale bars represent 10 µm.

Online Figure III

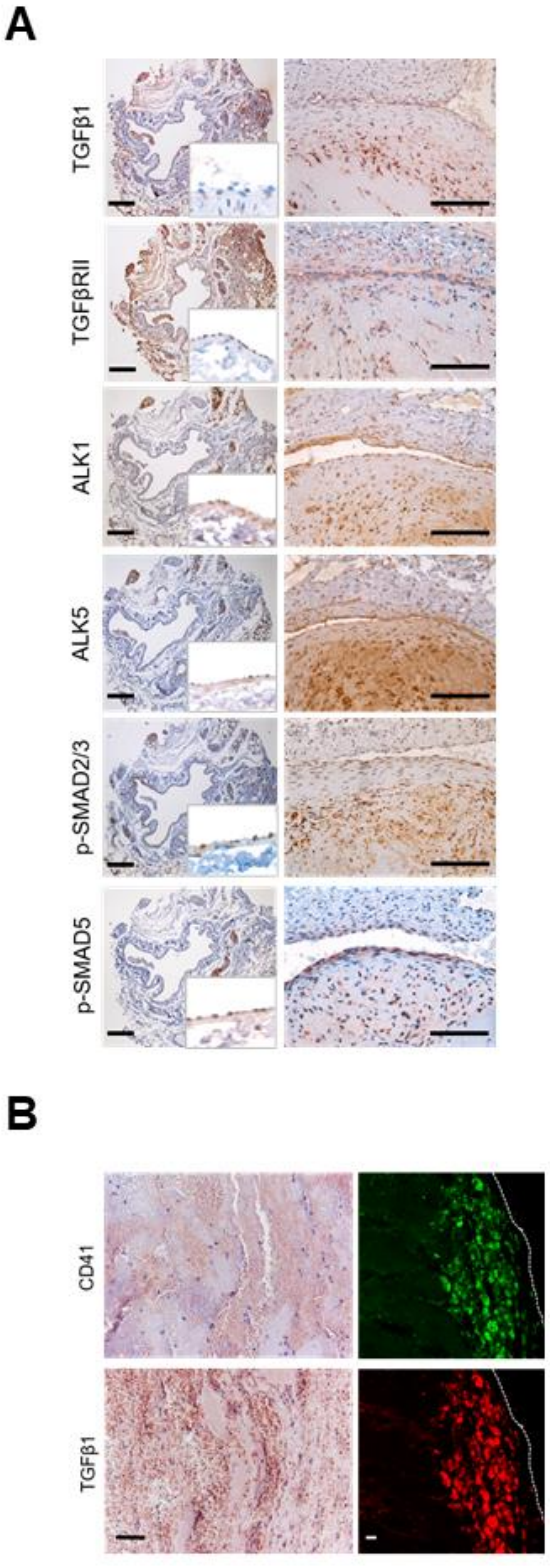

Online Figure III. Active TGFβ signaling during murine venous thrombus resolution. Representative images after immunohistochemical analysis of TGFβ1 and TGFβ signaling pathway components on serial cross-sections through the *inferior Vena cava* (IVC) obtained from C57BL/6 wild-type mice, uninjured and 21 days after IVC ligation (**A**). Representative pictures (n=3 independent experiments) show the expression of TGFβ1 and the TGFβ receptors TGFβRII, TGFβRI/ALK1, TGFβRI/ALK5 as well as phosphorylated SMAD2/3 and phosphorylated SMAD5 to visualize active TGFβ signaling. Scale bars represent 100 µm. Inserts show a higher magnification of selected areas of interest. Representative pictures (n=3 independent experiments) of immunohistochemical (left panel) and confocal fluorescence microscopy analysis (right panel) of mouse thrombi at day 7 after IVC ligation for CD41-positive platelets and TGFβ1 (**B**). Scale bars represent 10 µm.

Online Figure IV

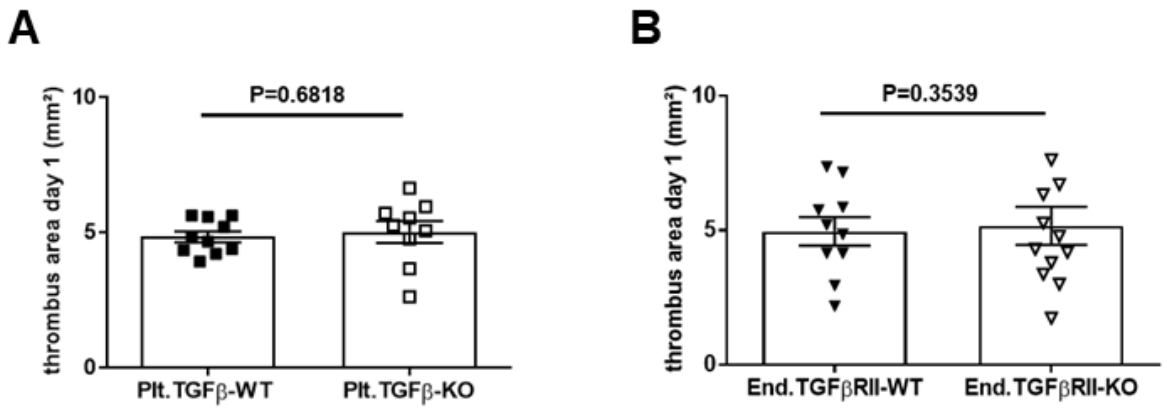

Online Figure IV. Venous thrombus area at day 1. Quantitative analysis of thrombus size (based on ultrasound findings) at day 1 after IVC ligation in Plt.TGFβ-WT and Plt.TGFβ-KO mice (n=10 in Plt.TGFβ-WT and n=9 in Plt.TGFβ-KO mice; P=0.6818) (**A**) and in End.TGFβRII-WT (n=10) and End.TGFβRII-KO (n=11; P=0.3539) mice (**B**) that developed a thrombus and were included in the study. Exact p-values, as determined by Student's t test, are shown.

Online Figure V

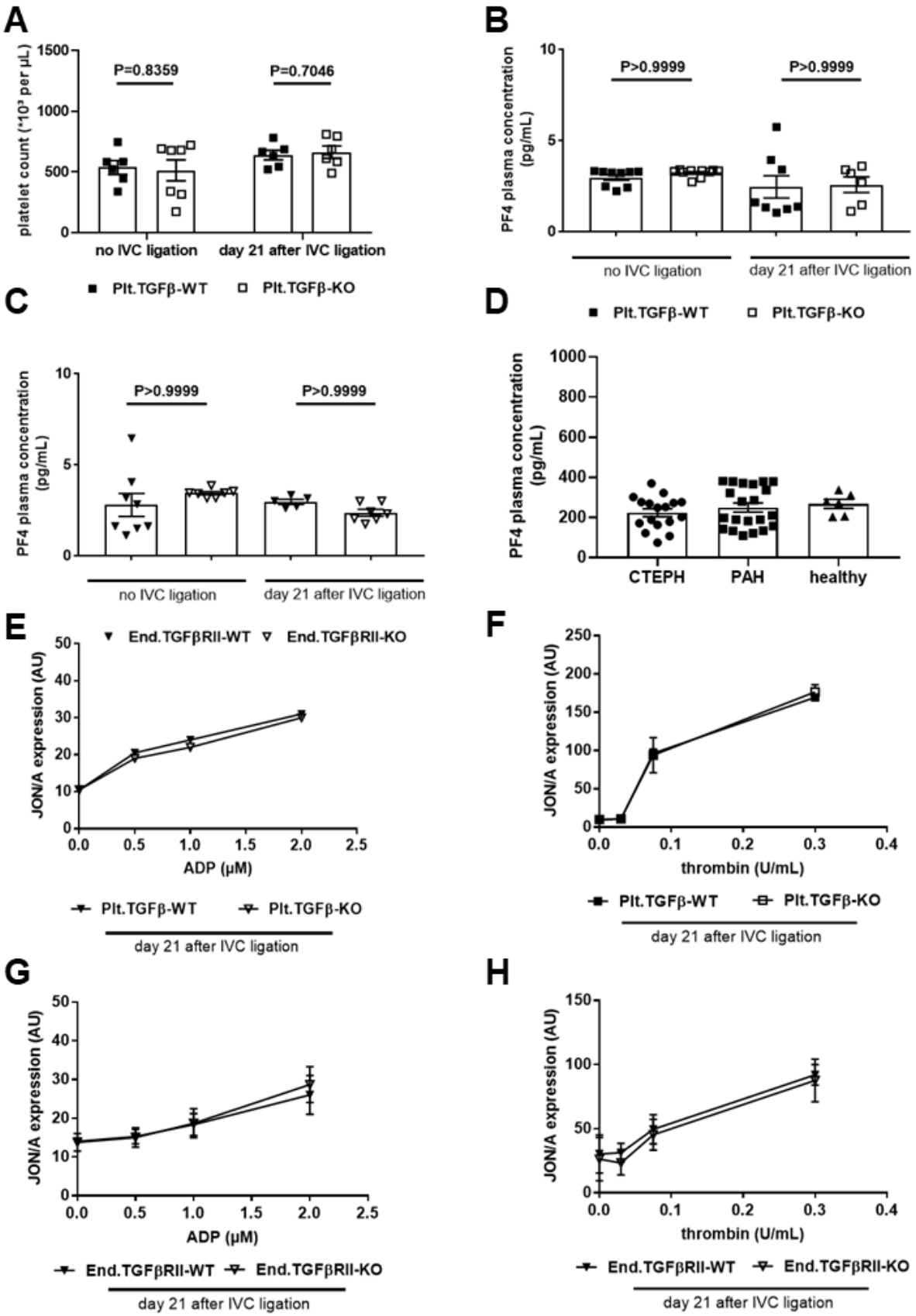

Online Figure V. Analysis of platelet counts and activated integrin αIIβ3 expression. Platelet counts in whole blood were determined in Plt.TGFβ-KO and Plt.TGFβ-WT mice, uninjured and at day 21 after IVC surgery (**A**; n=6-7 mice per group). Exact p-values, as determined by multiple t-test are shown. Plasma PF4 levels in Plt.TGFβ-KO vs. Plt.TGFβ-WT (**B**; n=9-10 uninjured mice and n=6-8 mice at day 21 after IVC ligation) and End.TGFβRII-KO vs. End.TGFβRII-WT mice (**C**; n=7-8 uninjured mice and n=5-7 at day 21 after IVC ligation). Exact p-values, as determined by multiple t-tests, are shown. Plasma PF4 levels in patients with CTEPH (n=17) and PAH (n=21) vs. healthy controls (n=6; **D**). Exact p-values were determined using One-Way ANOVA followed by Bonferroni's multiple comparisons test (3 comparisons). Non-significant p-values are not shown. Flow cytometry analysis of platelet-rich plasma for activated mouse integrin αIIβ3 (JON/A) expression in response to ADP or thrombin in Plt.TGFβ-KO vs. Plt.TGFβ-WT (**E** and **F**; n=3 per group) and in End.TGFβRII-KO vs. End.TGFβRII-WT (**G** and **H**; n=4 per group) mice.

Online Figure VI

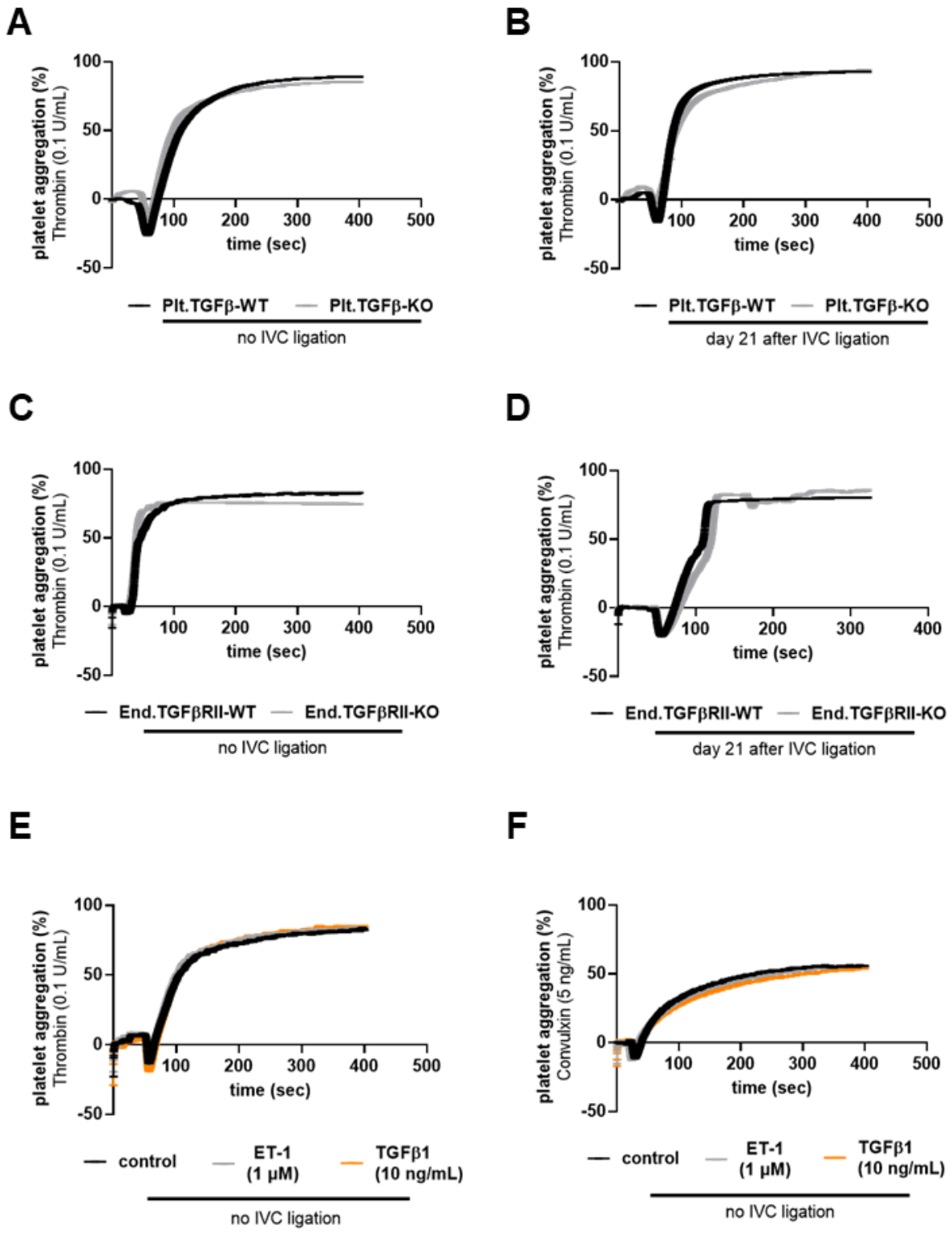

Online Figure VI. Analysis of platelet aggregation. Platelet-rich plasma isolated from Plt.TGFβ-WT and Plt.TGFβ-KO mice, uninjured (**A**) or at day 21 after IVC ligation (**B**), and from End.TGFβRII-WT and End.TGFβRII-KO mice, uninjured (**C**) or at day 21 after IVC ligation (**D**), was stimulated with thrombin (0.1 U/mL, in the presence of the fibrin-polymerization inhibiting peptide GPRP; n=3 independent experiments) and platelet aggregation recorded using light transmission aggregometry. Platelet-rich plasma isolated from C57BL/6J wild-type animals was pre-stimulated with ET-1 (1 μM) and TGFβ1 (10 ng/mL) for 10 min at 37°C followed by stimulation with thrombin (0.1 U/mL; **E**) or convulxin (**F**; 5 ng/mL; n=3 independent experiments per group) and platelet aggregation recorded using light transmission aggregometry. Representative aggregation tracings are shown.

Online Figure VII

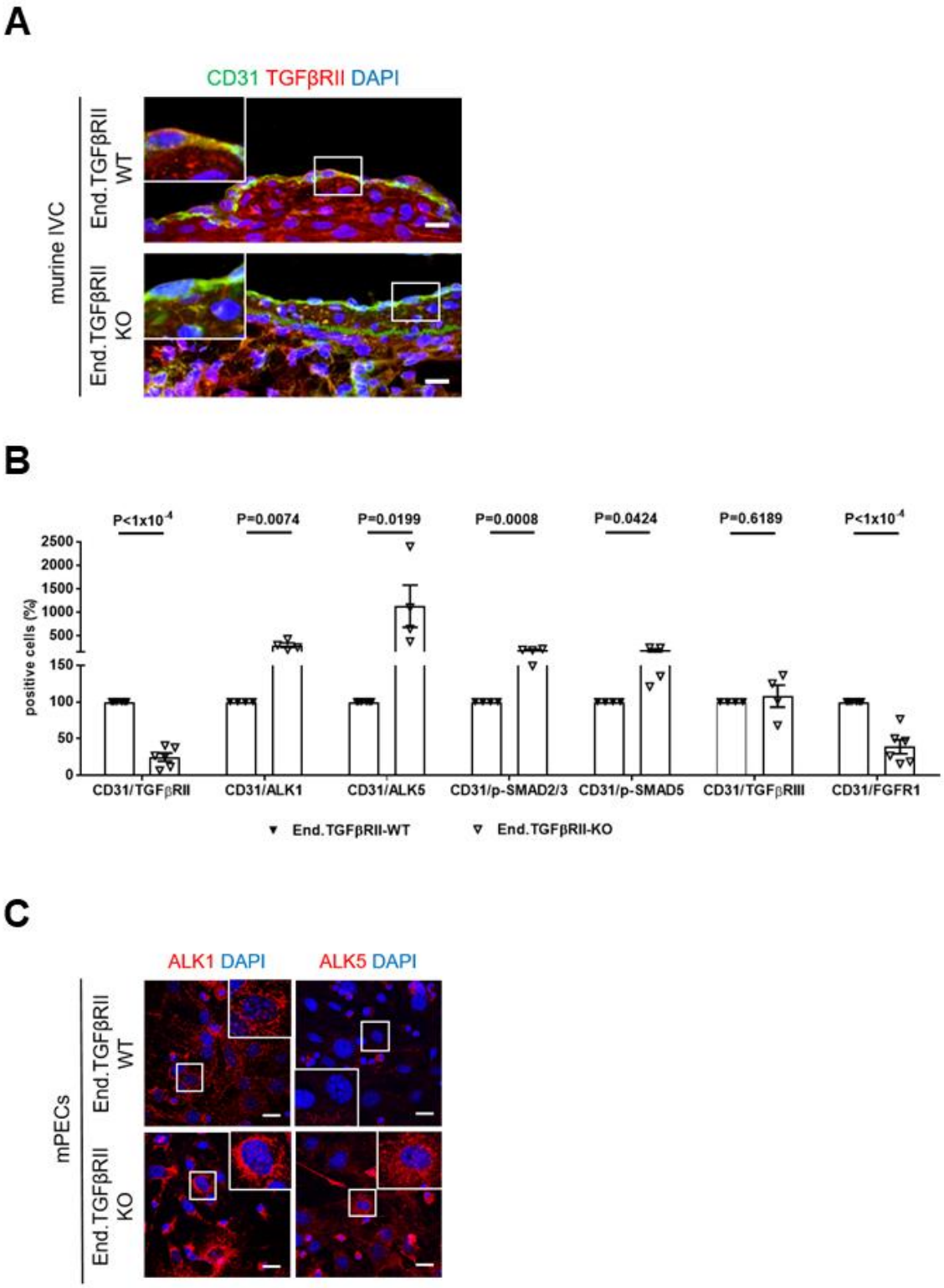

Online Figure VII. Expression of TGFβ receptors in endothelial cells of End.TGFβRII-WT and End.TGFβRII-KO mice. Representative confocal microscopy images of cryo-preserved cross-sections of the *inferior Vena cava* (IVC) 21 days after ligation immunostained for CD31 and TGFβRII (**A**; n=3 independent experiments). Scale bar represent 10 µm. Flow cytometry analysis and quantification of CD31-positive cells co-expressing TGFβRII, TGFβRI/ALK1, TGFβRI/ALK5, p-SMAD2/3, p-SMAD5, ~~and~~ TGFβRIII and FGFR1 (**B**; n=4-6 biological replicates). Findings in End.TGFβRII-WT and End.TGFβRII-KO mice were analyzed using multiple t-tests. Representative confocal microscopy images of primary murine endothelial cells (mPECs) isolated from lungs of End.TGFβRII-WT and End.TGFβRII-KO mice for ALK1 and ALK5 (**C**; n=3 independent experiments). Scale bars represent 10 µm. Inserts show higher magnification of selected areas of interest.

Online Figure VIII

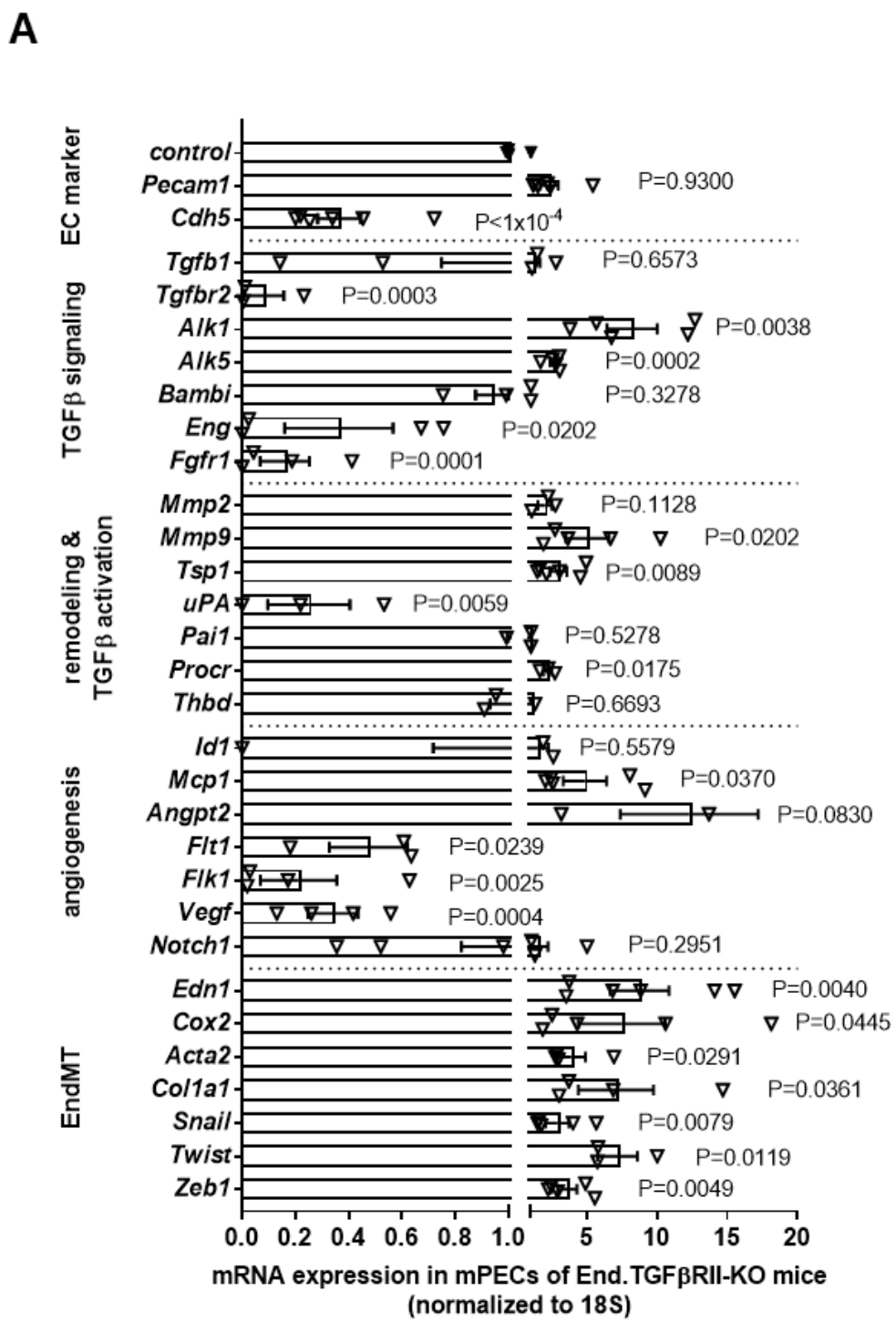

Online Figure VIII. *Ex vivo* gene expression profile of primary murine endothelial cells with genetic deletion of TGFβRII. Primary endothelial cells were isolated from lungs of End.TGFβRII-WT and End.TGFβRII-KO mice (n=3-6 per group), total RNA isolated and subjected to quantitative *real time* PCR analysis of endothelial cell (EC) markers (*Pecam1, Cdh5*), TGFβ signaling molecules (*Tgfb1, Tgfbr2, Alk1, Alk5, Bambi, Eng, Fgfr1*), remodeling and TGFβ activation (*Mmp2, Mmp9 ,Tsp1, uPA, Pai1, Procr, Thbd*), angiogenesis (*Id1, Mcp1, Angpt2, Flt1, Flk1, Vegf, Notch1*) and endothelial-to-mesenchymal transition (EndMT*; Edn1, Cox2, Acta2, Col1A1, Snail, Twist, Zeb1*). Values represent -fold change vs. values in End.TGFβRII-WT mice (control; set at 1) after normalization to 18S mRNA levels. Exact p-values were determined by Student's t-test.

Online Figure IX

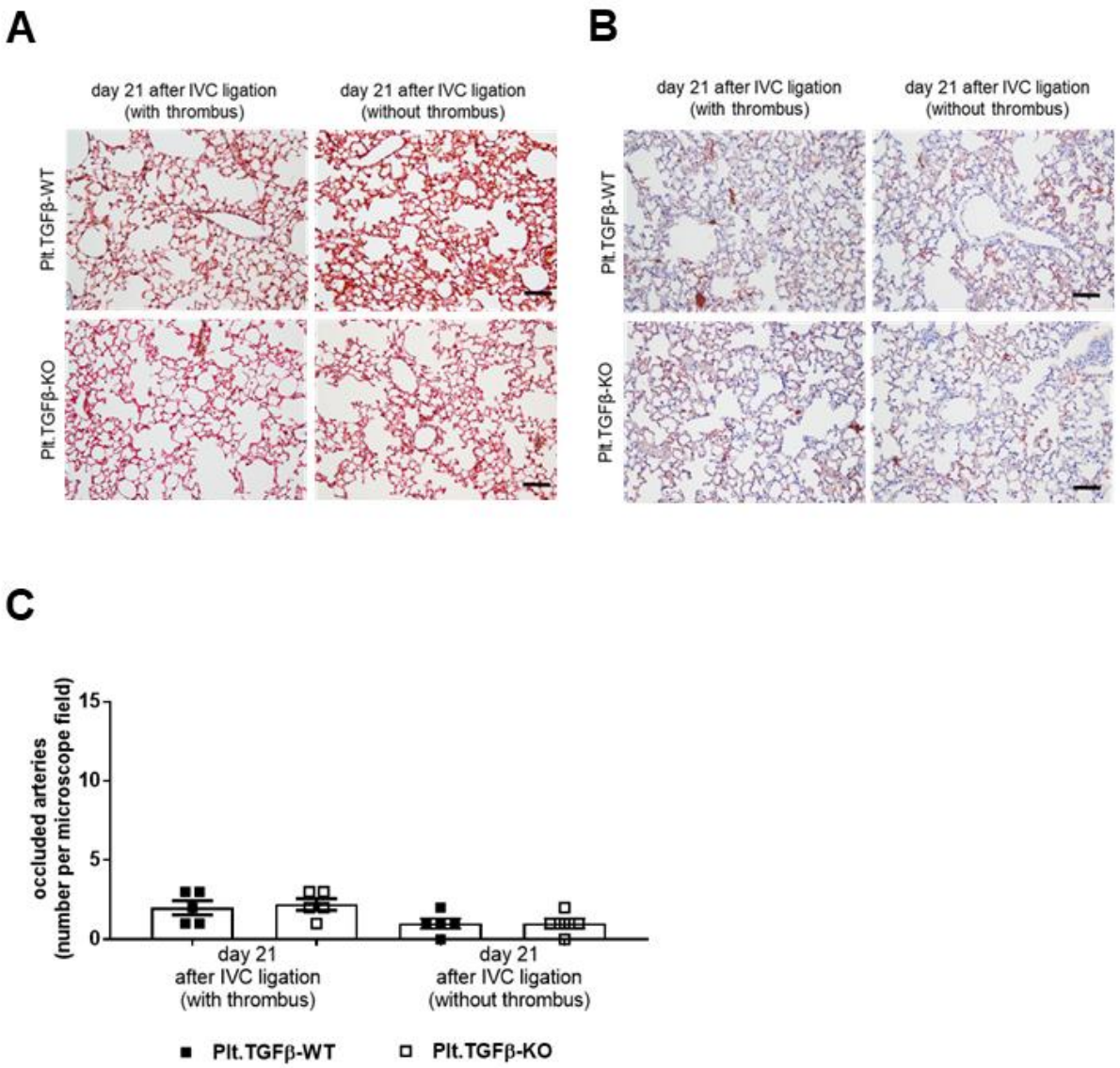

Online Figure IX. Pulmonary vascular occlusions following venous thrombosis in Plt.TGFβ mice. Representative images of PBS- and formalin-infused paraffin-embedded mouse lungs from Plt.TGFβ-WT and Plt.TGFβ-KO mice at day 21 after IVC ligation using Carstairs' staining (**A**) or immunostaining of fibrinogen (**B**; n=3 independent experiments). Scale bars represent 10 µm. The results of the quantitative analysis of red, fibrin-rich material in the pulmonary parenchyma are shown (n=5 mice per group; C). Exact p-values were determined by One-Way ANOVA followed by Bonferroni's multiple comparisons test (4 comparisons). Non-significant p-values are not shown.

Online Figure X

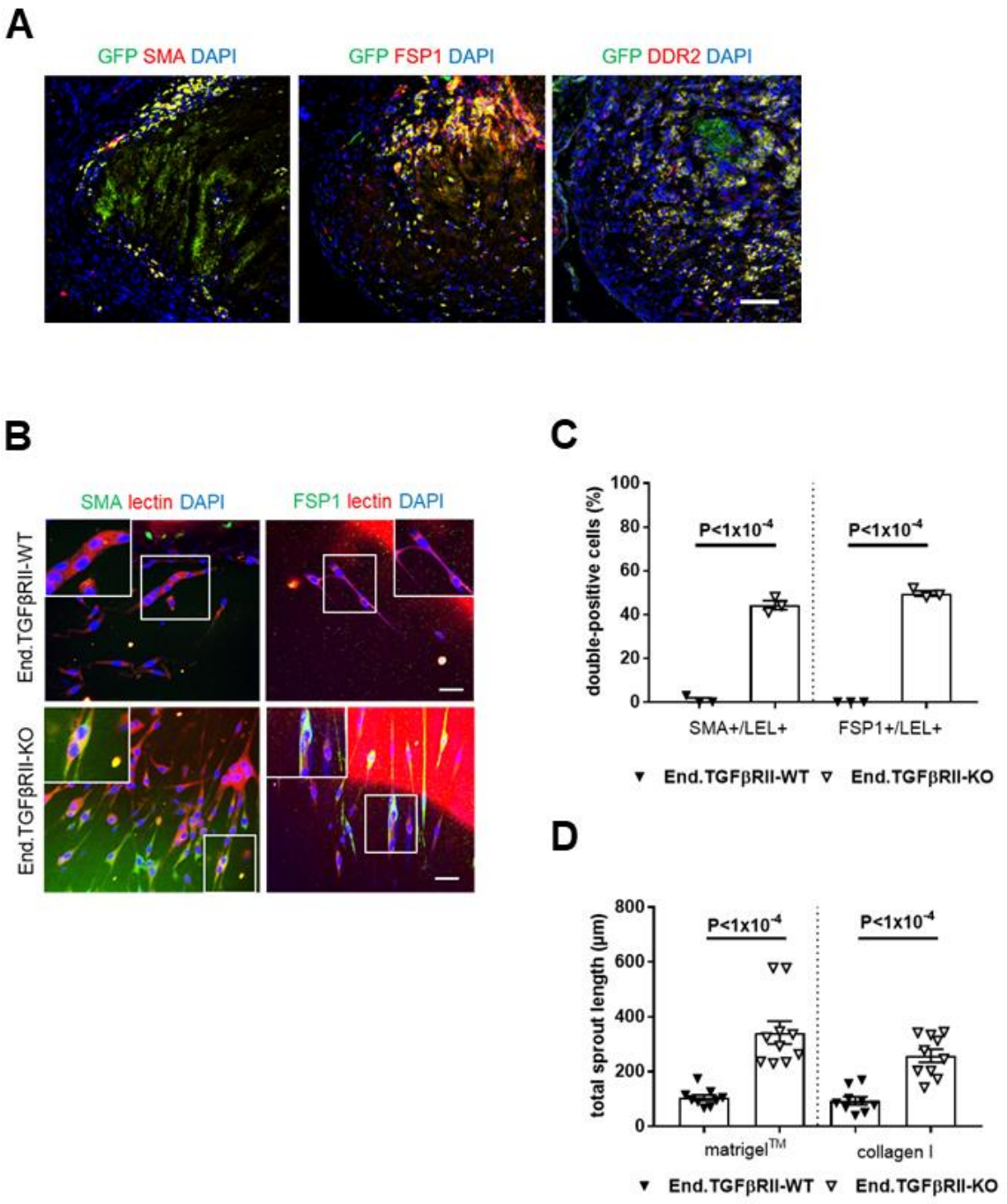

Online Figure X. Endothelial-to-mesenchymal transition during thrombus resolution and sprouting of endothelial cells. Representative confocal microscopy images of venous thrombi 21 days after IVC ligation in End.reporter mice (endothelial cells appear green) and immunostaining of mesenchymal markers (SMA, FSP1 and DDR2; red; n=3 independent experiments) (**A**). Dual-positive cells appear yellow. Cell nuclei are marked with DAPI (blue). Representative images (**B**) and the results of the quantitative analysis (**C**) of aortic rings isolated from End.TGFβRII-WT and End.TGFβRII-KO mice, cultured in matrigel™ and stained for mesenchymal (SMA and FSP1; green) and endothelial (LEL lectin; red) markers (n=3 independent experiments; $P<1x10^{-4}$ for both). Scale bar represents 10 µm. Quantitative analysis of total sprout length (**D;** n=4 independent experiments, $P<1x10^{-4}$ for both).

Online Figure XI

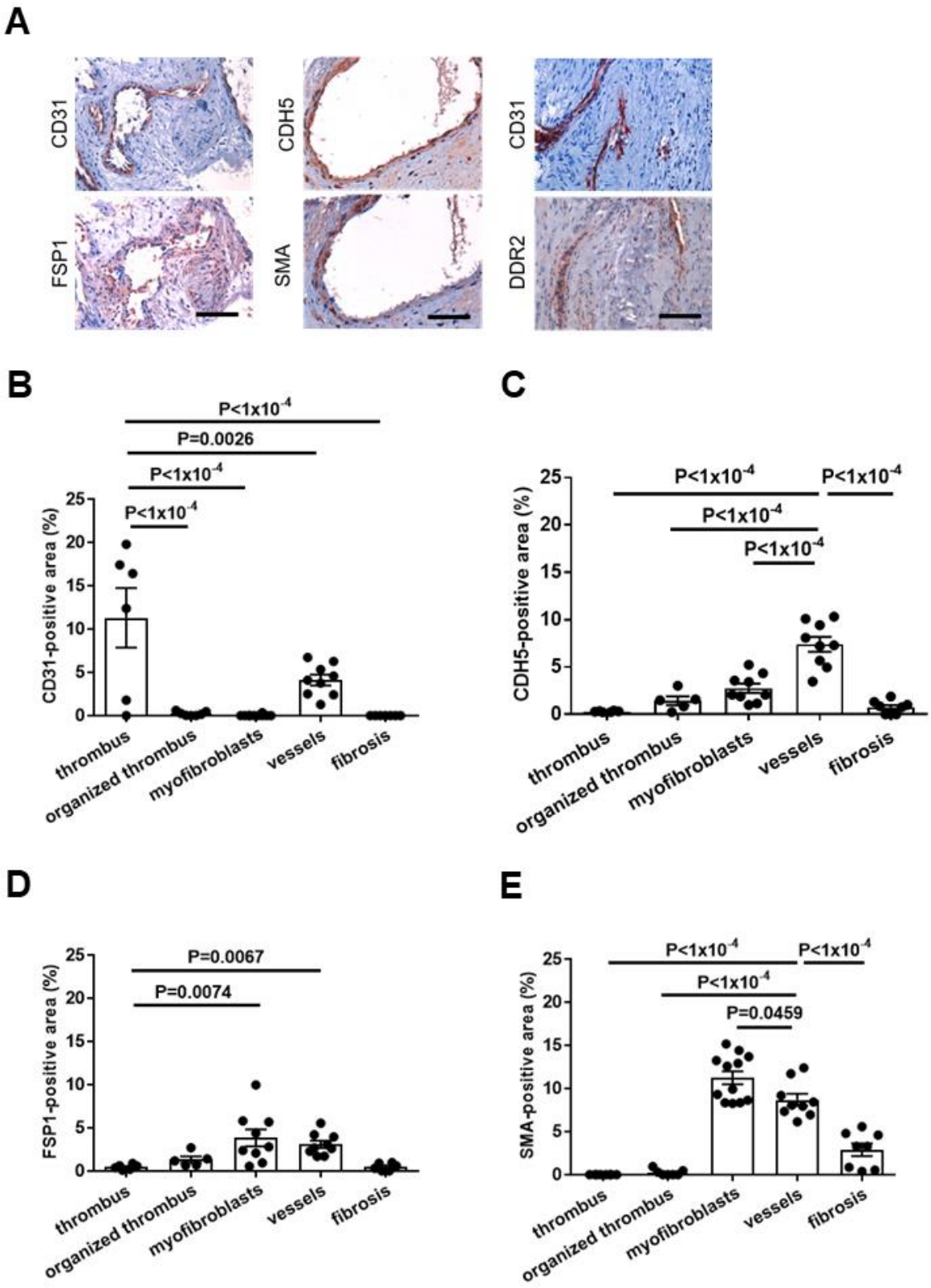

Online Figure XI. Immunostaining of endothelial and mesenchymal markers in pulmonary endarterectomy specimens. Representative images of vessel-rich areas within PEA tissue specimens of patients with CTEPH after immunostaining for endothelial (CD31, CDH5) or mesenchymal markers (FSP1, SMA, DDR2) (**A**) and the results of the quantitative analysis for the expression of CD31 (**B**), CDH5 (**C**) FSP1 (**D**) and SMA (**E**) in five pre-specified regions containing primarily fresh or organized thrombus, myofibroblasts, vessels or fibrosis (n=3 biological replicates). Scale bars represent 10 µm. Exact p-values, as determined by One-Way ANOVA followed by Bonferroni's multiple comparisons test (10 comparisons), are shown in panels B-E. Non-significant p-values are not shown.

Online Figure XII

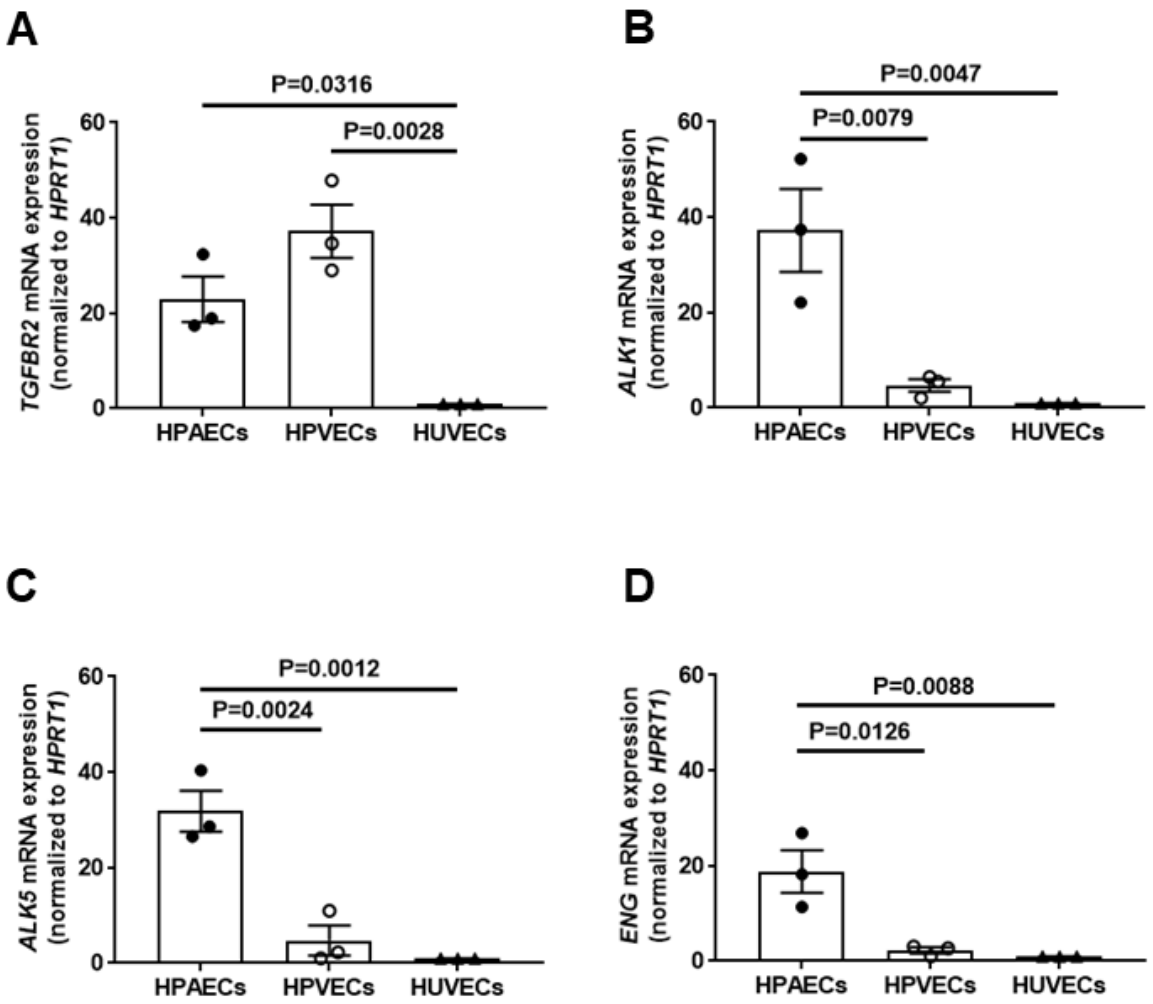

Online Figure XII. Expression of TGFβ receptors in human endothelial cells. The mRNA expression of TGFβRII (TGFBR2; **A**), ALK1 (**B**), ALK5 (**C**) and endoglin (ENG; **D**) was examined in human pulmonary arterial endothelial cells (HPAECs), human pulmonary vein endothelial cells (HPVECs) and human umbilical vein endothelial cells (HUVECs) using *real time* PCR (n=3 independent experiments). Data were normalized to the housekeeping gene HPRT1 and are expressed as -fold change vs. HUVECs (set at 1). Exact p-values were determined by One-Way ANOVA followed by Bonferroni's multiple comparisons test (3 comparisons). Non-significant p-values are not shown.

Online Figure XIII

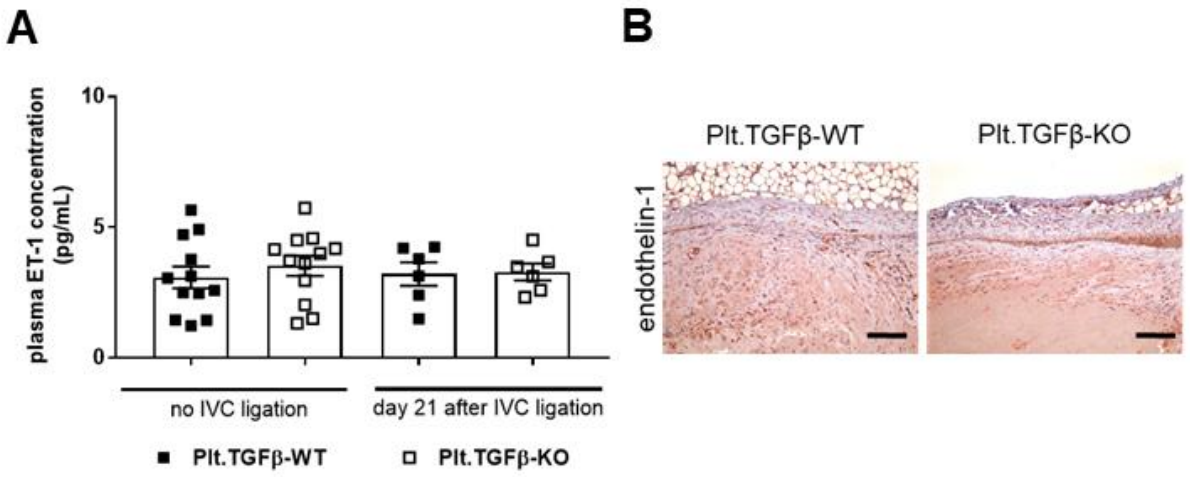

Online Figure XIII. Plasma and thrombus ET-1 level in Plt.TGFβ mice. Plasma levels of ET-1 in Plt.TGFβ-WT and Plt.TGFβ-KO mice, uninjured (n=12 mice per group) and at day 21 after IVC ligation (n=6 mice per group; **A**). Exact p-values were determined by One-Way ANOVA followed by Bonferroni's multiple comparisons test (4 comparisons). Non-significant p-values are not shown. Representative immunohistochemical images of mouse thrombi 21 days after IVC ligation stained for ET-1 in Plt.TGFβ-WT and Plt.TGFβ-KO mice (**B**; n=3 independent experiments).

Online Figure XIV

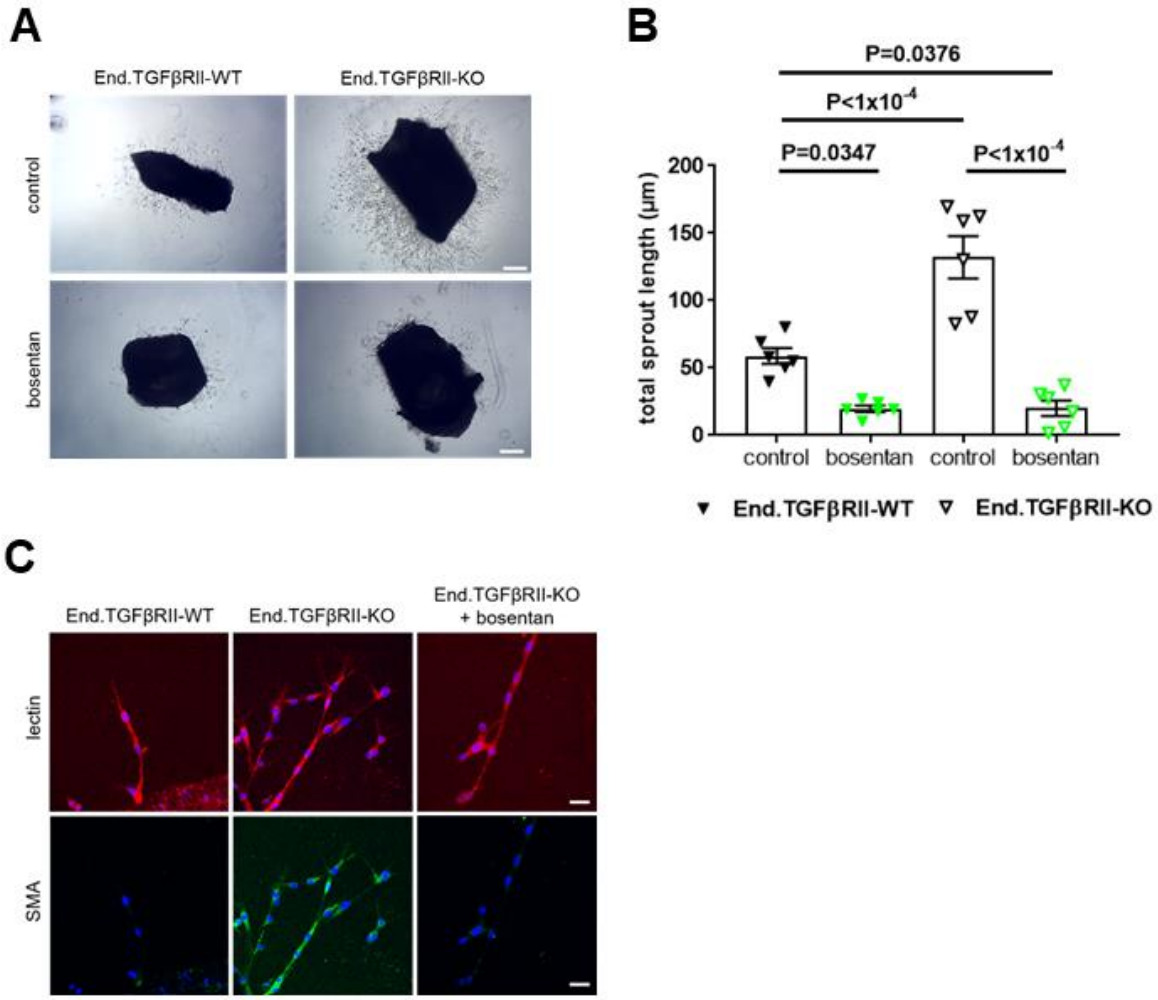

Online Figure XIV. Endothelial sprout formation: effects of endothelin-1 signaling inhibition. Representative brightfield pictures of aortic rings isolated from End.TGFβRII-WT and End.TGFβRII-KO mice and cultured in MV2 medium supplemented with bosentan (10 µM for 4 days) to block endothelin receptors (**A**; n=3 independent experiments). Total sprout length analysis of aortic rings isolated from End.TGFβRII-WT and End.TGFβRII-KO mice cultured in matrigel™ and treated with bosentan (labeled in green) (**B**; n=3 independent experiments, P=0.0347 for End.TGFβRII-WT and $P<1x10^{-4}$ for End.TGFβRII-KO). Exact p-values were determined by One-Way ANOVA followed by Bonferroni's multiple comparisons test (4 comparisons). Representative confocal pictures of aortic rings isolated from End.TGFβRII-WT and End.TGFβRII-KO mice and stained with endothelial lectin (red) and SMA (green) with and without treatment with bosentan (10 µM for 7 days). Scale bars represent 10 µm. (**C**; n=4 independent experiments).

Online Figure XV

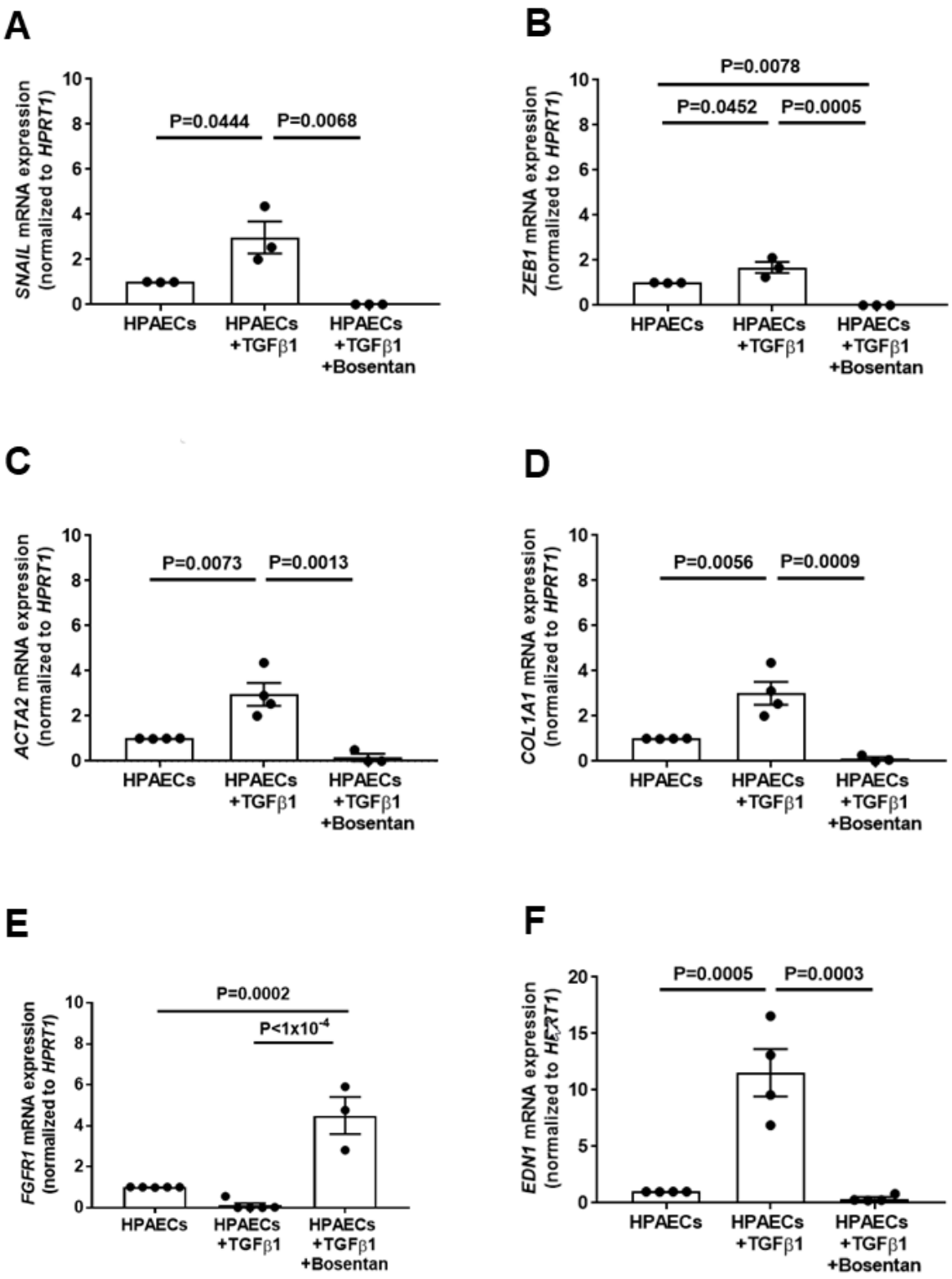

Online Figure XV. Gene expression of transcriptional regulators of endothelial-to-mesenchymal transition and mesenchymal markers in human pulmonary endothelial cells. Quantitative *real time* PCR analysis and comparison of mRNA expression levels of the transcriptional regulators SNAIL (**A**; n=3 independent experiments) and ZEB1 (**B**; n=3 independent experiments), the mesenchymal markers smooth muscle α-actin (ACTA2; **C**; n=4 independent experiments) and collagen 1A1 (COL1A1; **D**; n=4 independent experiments), the repressor of TGFβ signaling in endothelial cell FGFR1 (**E**; n=3-5 independent experiments) and of endothelin-1 (EDN1; **F**; n=4 independent experiments) in Human Pulmonary Artery Endothelial Cells (HPAECs) with and without stimulation for 7 days with TGFβ1 (10 ng/mL) and bosentan (10 μM). Values were normalized to the housekeeping gene HPRT1 and are expressed as -fold change vs. HPAECs (set at 1). Exact p-values were determined by One-Way ANOVA followed by Bonferroni's multiple comparisons test (3 comparisons). Non-significant p-values are not shown.

Online Figure XVI

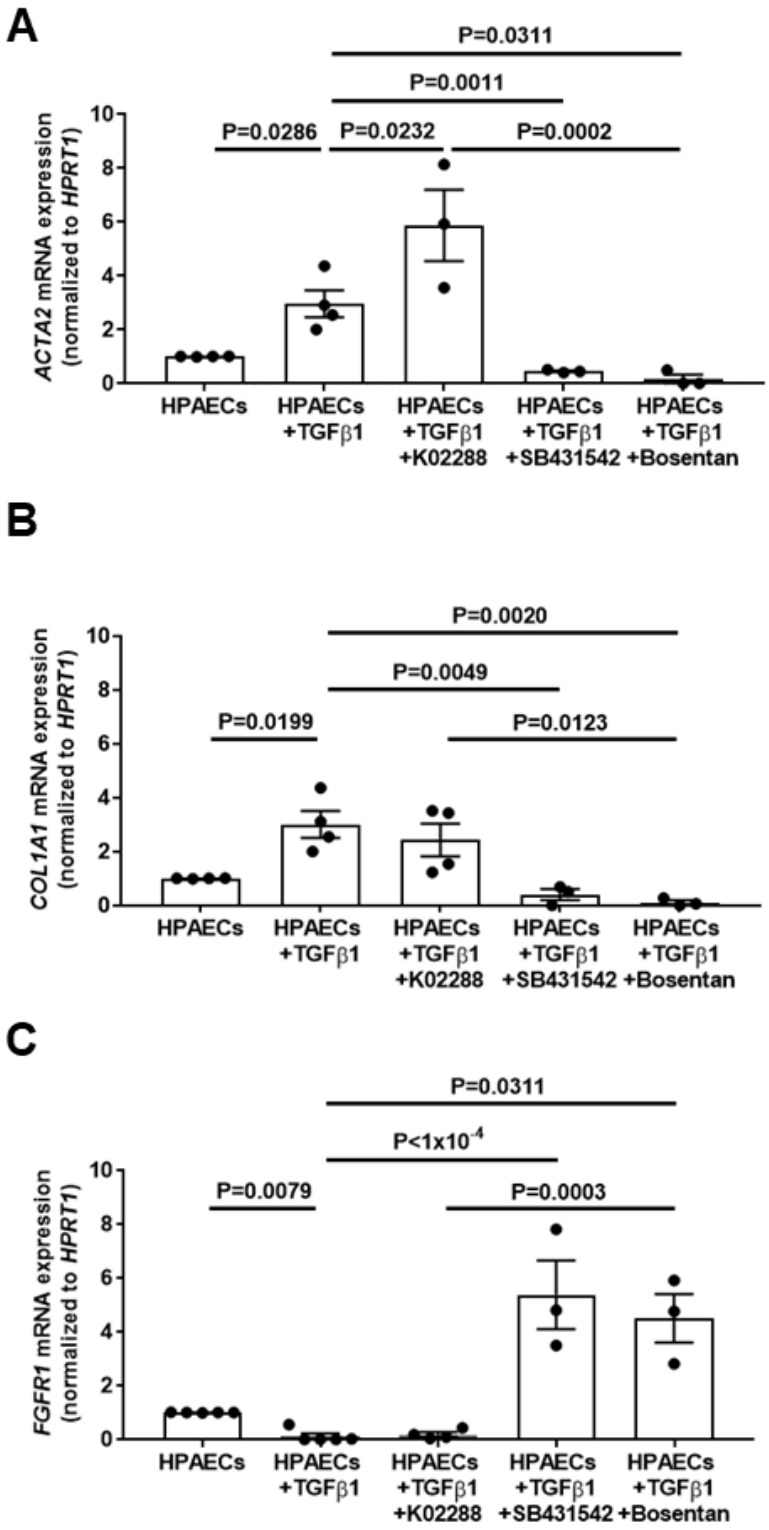

Online Figure XVI. Expression of ACTA2, COL1A1 and FGFR1 in human primary endothelial cells: effects of TGFβ1 stimulation and TGFβRI signaling inhibition or ET-1 antagonization. The mRNA expression of ACTA2 (**A**), COL1A1 (**B**) and FGFR1 (**C**) was examined in human pulmonary arterial endothelial cells (HPAECs) using *real time* PCR analysis (n=3-5 independent experiments). HPAECs were treated with TGFβ1 (10 ng/mL) and K02288 (10 μM), SB431542 (10 μM) or bosentan (10 μM) to inhibit TGFβRI/ALK1, TGFβRI/ALK5 and endothelin signaling, respectively. Data were normalized to housekeeping gene HPRT1 and are expressed as -fold change vs. HPAECs (set at 1). Exact p-values were determined by One-Way ANOVA followed by Bonferroni's multiple comparisons test (7 comparisons). Non-significant p-values are not shown.

Online Figure XVII

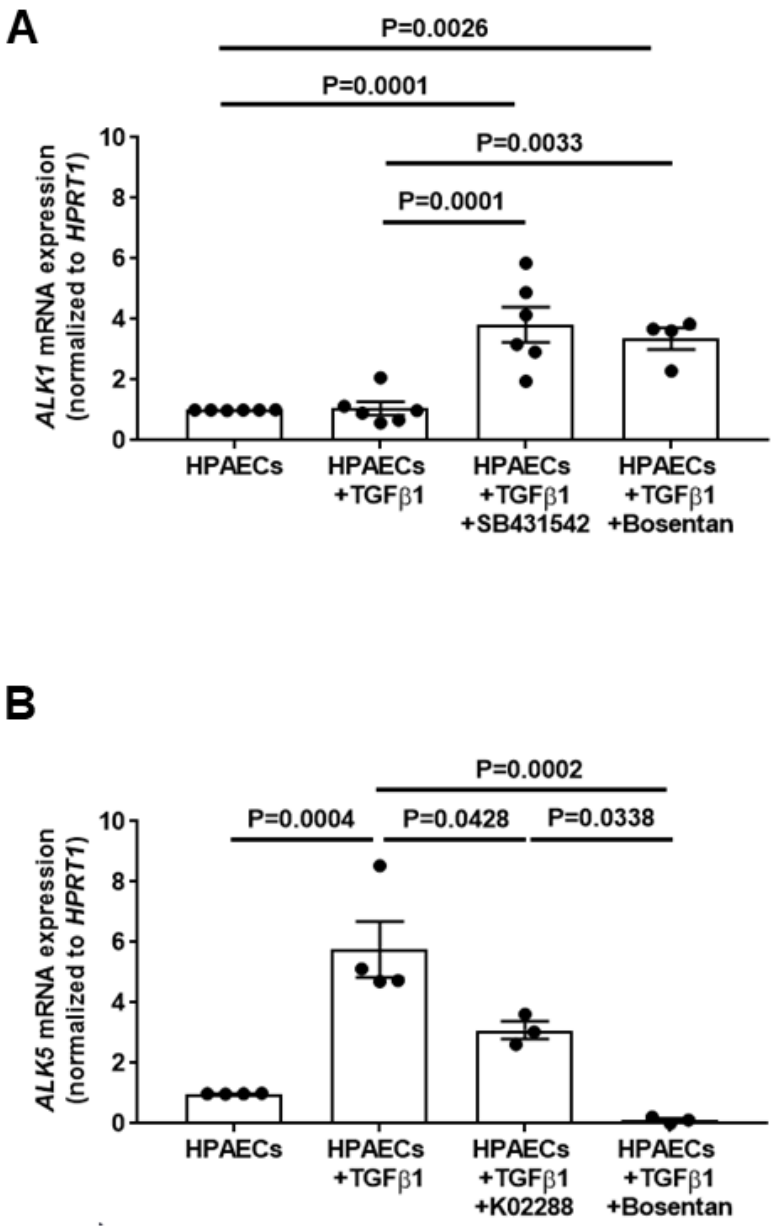

Online Figure XVII. Expression of ALK1 and ALK5 in human primary endothelial cells: effects of TGFβ1 stimulation or TGFβRI signaling inhibition. The mRNA expression of ALK1 (**A**; n=4-6 independent experiments) and ALK5 (**B**; n=3-4 independent experiments) was examined in human pulmonary arterial endothelial cells (HPAECs) using *real time* PCR analysis. Cells were treated with TGFβ1 (10 ng/mL) and K02288 (10 μM), SB431542 (10 μM) or bosentan (10 μM) to inhibit TGFβRI/ALK1, TGFβRI/ALK5 and endothelin signaling, respectively. Data were normalized to the housekeeping gene HPRT1 and are expressed as -fold change vs. HPAECs (set at 1). Exact p-values were determined using One-Way ANOVA followed by Bonferroni's multiple comparisons test (6 comparisons). Non-significant p-values are not shown.

Online Figure XVIII

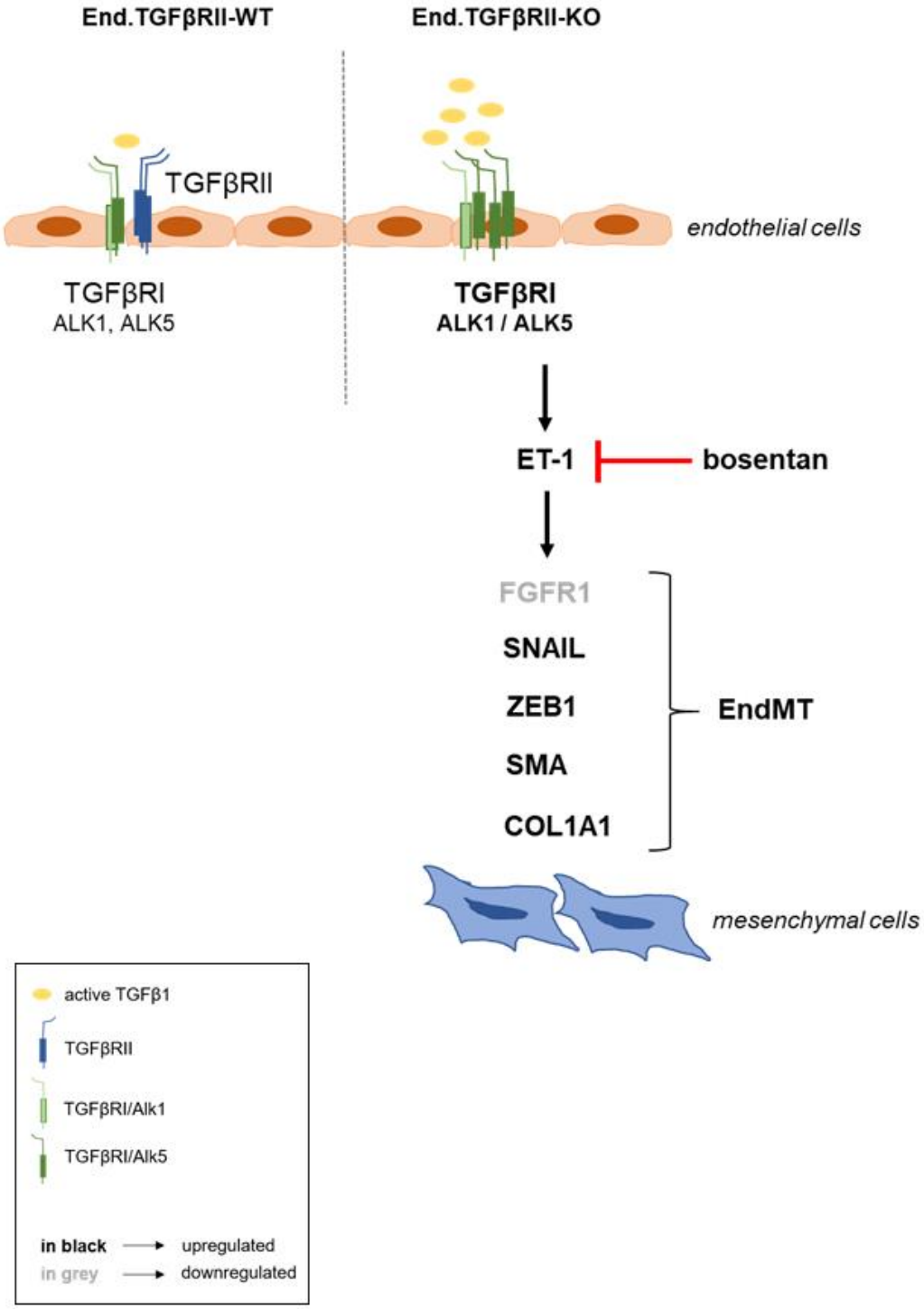

Online Figure XVIII. Schematic drawing of activated TGFβ1 signaling in endothelial cells through TGFβRI and endothelin-1 and its role in thrombofibrosis.

Supplemental References

1. Azhar M, Yin M, Bommireddy R, Duffy JJ, Yang J, Pawlowski SA, Boivin GP, Engle SJ, Sanford LP, Grisham C, Singh RR, Babcock GF, Doetschman T. Generation of mice with a conditional allele for transforming growth factor beta 1 gene. *Genesis*. 2009;47:423-431.
2. Cazac BB, Roes J. Tgf-beta receptor controls b cell responsiveness and induction of iga in vivo. *Immunity*. 2000;13:443-451.
3. Forde A, Constien R, Grone HJ, Hammerling G, Arnold B. Temporal cre-mediated recombination exclusively in endothelial cells using tie2 regulatory elements. *Genesis*. 2002;33:191-197.
4. Jäger M, Hubert A, Gogiraju R, Bochenek ML, Münzel T, Schäfer K. Inducible knockdown of endothelial protein tyrosine phosphatase-1b promotes neointima formation in obese mice by enhancing endothelial senescence. *Antioxid Redox Signal*. 2018.
5. Bochenek ML, Bauer T, Gogiraju R, Nadir Y, Mann A, Schönfelder T, Hünig L, Brenner B, Münzel T, Wenzel P, Konstantinides S, Schäfer K. The endothelial tumor suppressor p53 is essential for venous thrombus formation in aged mice. *Blood Adv*. 2018;2:1300-1314.
6. Caires A, Fernandes GS, Leme AM, Castino B, Pessoa EA, Fernandes SM, Fonseca CD, Vattimo MF, Schor N, Borges FT. Endothelin-1 receptor antagonist protect the kidney against the nephrotoxicity induced by cyclosporine-A in normotensive rats. *Braz J Med Biol Res*. 2018;51.
7. Zuo WL, Zhao JM, Huang JX, Zhou W, Lei ZH, Huang YM, Huang YF, Li HG. Effect of bosentan is correlated with MMP9/TIMP-1 ratio in bleomycin-induced pulmonary fibrosis. *Biom Rep*. 2017;6:201-205.

8. Brandt M, Giokoglu E, Garlapati V, Bochenek ML, Molitor M, Hobohm L, Schönfelder T, Münzel T, Kossmann S, Karbach SH, Schäfer K, Wenzel P. Pulmonary arterial hypertension and endothelial dysfunction is linked to nadph oxidase-derived superoxide formation in venous thrombosis and pulmonary embolism in mice. *Oxid Med Cell Longev*. 2018;2018:1860513.
9. Baker M, Robinson SD, Lechertier T, Barber PR, Tavora B, D'Amico G, Jones DT, Vojnovic B, Hodivala-Dilke K. Use of the mouse aortic ring assay to study angiogenesis. *Nat Protoc*. 2011;7:89-104.
10. Mori Y, Ishida W, Bhattacharyya S, Li Y, Platanias LC, Varga J. Selective inhibition of activin receptor-like kinase 5 signaling blocks profibrotic transforming growth factor beta responses in skin fibroblasts. *Arthritis Rheum*. 2004;50:4008-4021.
11. Kerr G, Sheldon H, Chaikuad A, Alfano I, von Delft F, Bullock AN, Harris AL. A small molecule targeting alk1 prevents notch cooperativity and inhibits functional angiogenesis. *Angiogenesis*. 2015;18:209-217.
12. Subramaniam S, Jurk K, Hobohm L, Jäckel S, Saffarzadeh M, Swierczek K, Wenzel P, Langer F, Reinherdt C, Ruf W. Distinct contributions of complement factors to platelet activation and fibrin formation in venous thrombus development. *Blood*. 2017;129:2291-2302.
13. Frenette PS, Denis CV, Weiss L, Jurk K, Subbarao S, Kehrel B, Hartwig JH, Vestweber D, Wagner DD. P-Selectin glycoprotein ligand 1 (PSGL-1) is expressed on platelets and can mediate platelet-endothelial interactions in vivo. *J Exp Med*. 2000;191:1413-1422.
14. Steven S, Jurk K, Kopp M, Kröller-Schön S, Mikhed Y, Swierczek K, Roohani S, Kashani F, Oelze M, Klein T, Tokalov S, Danckwardt S, Strand S, Wenzel P, Münzel T, Daiber A. Glucagon-like peptide-1 receptor signaling reduces microvascular

thrombosis, nitro-oxidative stress and platelet activation in endotoxaemic mice. *Br J Pharmacol*. 2017;174:1620-1632.

15. Bochenek ML, Rosinus NS, Lankeit M, Hobohm L, Bremmer F, Schütz E, Klok FA, Horke S, Wiedenroth CB, Münzel T, Lang IM, Mayer E, Konstantinides S, Schäfer K. From thrombosis to fibrosis in chronic thromboembolic pulmonary hypertension. *Thromb Haemost*. 2017;117:769-783.
16. Tiedt R, Schomber T, Hao-Shen H, Skoda RC. Pf4-cre transgenic mice allow the generation of lineage-restricted gene knockouts for studying megakaryocyte and platelet function in vivo. *Blood*. 2007;109:1503-1506.
17. De Gasperi R, Rocher AB, Sosa MA, Wearne SL, Perez GM, Friedrich VL, Jr., Hof PR, Elder GA. The irg mouse: A two-color fluorescent reporter for assessing cre-mediated recombination and imaging complex cellular relationships in situ. *Genesis*. 2008;46:308-317.
18. Wicks J, Haitchi HM, Holgate ST, Davies DE, Powell RM. Enhanced upregulation of smooth muscle related transcripts by tgf beta2 in asthmatic (myo) fibroblasts. *Thorax*. 2006;61:313-319
19. Young K, Conley B, Romero D, Tweedie E, O'Neill C, Pinz I, Brogan L, Lindner V, Liaw L, Vary CP. Bmp9 regulates endoglin-dependent chemokine responses in endothelial cells. *Blood*. 2012;120:4263-4273.
20. Yao Y, Zebboudj AF, Torres A, Shao E, Bostrom K. Activin-like kinase receptor 1 (alk1) in atherosclerotic lesions and vascular mesenchymal cells. *Cardiovasc Res*. 2007;74:279-289.
21. Mao XG, Xue XY, Wang L, Zhang X, Yan M, Tu YY, Lin W, Jiang XF, Ren HG, Zhang W, Song SJ. Cdh5 is specifically activated in glioblastoma stemlike cells and contributes to vasculogenic mimicry induced by hypoxia. *Neuro Oncol*. 2013;15:865-879.

22. Goldberg SR, Quirk GL, Sykes VW, Kordula T, Lanning DA. Altered procollagen gene expression in mid-gestational mouse excisional wounds. *J Surg Res*. 2007;143:27-34.

23. Yuan W, Zhao MD, Yuan FL, Che W, Duan PG, Liu Y, Dong J. Association of endothelin-1 expression and cartilaginous endplate degeneration in humans. *PLoS One*. 2013;8:e60062.

24. Blanco FJ, Grande MT, Langa C, Oujo B, Velasco S, Rodriguez-Barbero A, Perez-Gomez E, Quintanilla M, Lopez-Novoa JM, Bernabeu C. S-endoglin expression is induced in senescent endothelial cells and contributes to vascular pathology. *Circ Res*. 2008;103:1383-1392.

25. Yan D, Chen D, Cool SM, van Wijnen AJ, Mikecz K, Murphy G, Im HJ. Fibroblast growth factor receptor 1 is principally responsible for fibroblast growth factor 2-induced catabolic activities in human articular chondrocytes. *Arthritis Res Ther*. 2011;13:R130.

26. Galiveti CR, Rozhdestvensky TS, Brosius J, Lehrach H, Konthur Z. Application of housekeeping npcrnas for quantitative expression analysis of human transcriptome by real-time pcr. *RNA*. 2010;16:450-461.

27. Behr B, Tang C, Germann G, Longaker MT, Quarto N. Locally applied vascular endothelial growth factor a increases the osteogenic healing capacity of human adipose-derived stem cells by promoting osteogenic and endothelial differentiation. *Stem Cells*. 2011;29:286-296.

28. Xu X, Tan X, Tampe B, Sanchez E, Zeisberg M, Zeisberg EM. Snail is a direct target of hypoxia-inducible factor 1alpha (hif1alpha) in hypoxia-induced endothelial to mesenchymal transition of human coronary endothelial cells. *J Biol Chem*. 2015;290:16653-16664.

29. Xie S, Macedo P, Hew M, Nassenstein C, Lee KY, Chung KF. Expression of transforming growth factor-beta (tgf-beta) in chronic idiopathic cough. *Respir Res*. 2009;10:40.

30. da Silveira JC, Carnevale EM, Winger QA, Bouma GJ. Regulation of acvr1 and id2 by cell-secreted exosomes during follicle maturation in the mare. *Reprod Biol Endocrinol*. 2014;12:44.

31. Zhu J, Huang Z, Zhang M, Wang W, Liang H, Zeng J, Wu K, Wang X, Hsieh JT, Guo P, Fan J. Hif-1alpha promotes zeb1 expression and emt in a human bladder cancer lung metastasis animal model. *Oncol Lett*. 2018;15:3482-3489.

32. Wang R, Guo YL. Transient inhibition of cell proliferation does not compromise self-renewal of mouse embryonic stem cells. *Exp Cell Res*. 2012;318:2094-2104.

33. Luo J, Tang M, Huang J, He BC, Gao JL, Chen L, Zuo GW, Zhang W, Luo Q, Shi Q, Zhang BQ, Bi Y, Luo X, Jiang W, Su Y, Shen J, Kim SH, Huang E, Gao Y, Zhou JZ, Yang K, Luu HH, Pan X, Haydon RC, Deng ZL, He TC. Tgfbeta/bmp type i receptors alk1 and alk2 are essential for bmp9-induced osteogenic signaling in mesenchymal stem cells. *J Biol Chem*. 2010;285:29588-29598.

34. Fan Y, Li X, Xiao W, Fu J, Harris RC, Lindenmeyer M, Cohen CD, Guillot N, Baron MH, Wang N, Lee K, He JC, Schlondorff D, Chuang PY. Bambi elimination enhances alternative tgf-beta signaling and glomerular dysfunction in diabetic mice. *Diabetes*. 2015;64:2220-2233.

35. Meadows KN, Iyer S, Stevens MV, Wang D, Shechter S, Perruzzi C, Camenisch TD, Benjamin LE. Akt promotes endocardial-mesenchyme transition. *J Angiogenes Res*. 2009;1:2.

36. Zeisberg EM, Tarnavski O, Zeisberg M, Dorfman AL, McMullen JR, Gustafsson E, Chandraker A, Yuan X, Pu WT, Roberts AB, Neilson EG, Sayegh MH, Izumo S,

Kalluri R. Endothelial-to-mesenchymal transition contributes to cardiac fibrosis. *Nat Med*. 2007;13:952-961.

37. Heiden S, Vignon-Zellweger N, Masuda S, Yagi K, Nakayama K, Yanagisawa M, Emoto N. Vascular endothelium derived endothelin-1 is required for normal heart function after chronic pressure overload in mice. *PLoS One*. 2014;9:e88730.

38. Kurosu H, Choi M, Ogawa Y, Dickson AS, Goetz R, Eliseenkova AV, Mohammadi M, Rosenblatt KP, Kliewer SA, Kuro-o M. Tissue-specific expression of betaklotho and fibroblast growth factor (fgf) receptor isoforms determines metabolic activity of fgf19 and fgf21. *J Biol Chem*. 2007;282:26687-26695.

39. Papaspyridonos M, Matei I, Huang Y, do Rosario Andre M, Brazier-Mitouart H, Waite JC, Chan AS, Kalter J, Ramos I, Wu Q, Williams C, Wolchok JD, Chapman PB, Peinado H, Anandasabapathy N, Ocean AJ, Kaplan RN, Greenfield JP, Bromberg J, Skokos D, Lyden D. Id1 suppresses anti-tumour immune responses and promotes tumour progression by impairing myeloid cell maturation. *Nat Commun*. 2015;6:6840.

40. Padilla J, Jenkins NT, Thorne PK, Lansford KA, Fleming NJ, Bayless DS, Sheldon RD, Rector RS, Laughlin MH. Differential regulation of adipose tissue and vascular inflammatory gene expression by chronic systemic inhibition of nos in lean and obese rats. *Physiol Rep*. 2014;2:e00225.

41. Vaillant B, Chiaramonte MG, Cheever AW, Soloway PD, Wynn TA. Regulation of hepatic fibrosis and extracellular matrix genes by the th response: New insight into the role of tissue inhibitors of matrix metalloproteinases. *J Immunol*. 2001;167:7017-7026.

42. Bansal K, Kapoor N, Narayana Y, Puzo G, Gilleron M, Balaji KN. Pim2 induced cox-2 and mmp-9 expression in macrophages requires pi3k and notch1 signaling. *PLoS One*. 2009;4:e4911.

43. Syed KM, Joseph S, Mukherjee A, Majumder A, Teixeira JM, Dutta D, Pillai MR. Histone chaperone aplf regulates induction of pluripotency in murine fibroblasts. *J Cell Sci*. 2016;129:4576-4591.

44. Kumar S, Shah S, Tang HM, Smith M, Borras T, Danias J. Tissue plasminogen activator in trabecular meshwork attenuates steroid induced outflow resistance in mice. *PLoS One*. 2013;8:e72447.

45. Okada H, Kikuta T, Kobayashi T, Inoue T, Kanno Y, Takigawa M, Sugaya T, Kopp JB, Suzuki H. Connective tissue growth factor expressed in tubular epithelium plays a pivotal role in renal fibrogenesis. *J Am Soc Nephrol: JASN*. 2005;16:133-143.

46. Diaz-Chavez J, Hernandez-Pando R, Lambert PF, Gariglio P. Down-regulation of transforming growth factor-beta type ii receptor (tgf-betarii) protein and mrna expression in cervical cancer. *Mol Cancer*. 2008;7:3.

47. McEachron TA, Pawlinski R, Richards KL, Church FC, Mackman N. Protease-activated receptors mediate crosstalk between coagulation and fibrinolysis. *Blood*. 2010;116:5037-5044.

48. Renthal NE, Chen CC, Williams KC, Gerard RD, Prange-Kiel J, Mendelson CR. Mir-200 family and targets, zeb1 and zeb2, modulate uterine quiescence and contractility during pregnancy and labor. *Proc Natl Acad Sci U S A*. 2010;107:20828-20833.